WT-1313 (EX)

EXTRACTED VERSION

OPERATION REDWING

Project 2.51
Neutron-Flux Measurements

Pacific Proving Grounds
May — July 1956

Headquarters Field Command
Defense Atomic Support Agency
Sandia Base, Albuquerque, New Mexico

September 30, 1959

NOTICE

This is an extract of WT-1313, Operation REDWING, Project 2.51, which remains classified SECRET/RESTRICTED DATA as of this date.

Extract version prepared for:

Director
DEFENSE NUCLEAR AGENCY
Washington, D.C. 20305

15 May 1981

Approved for public release distribution unlimited.

UNCLASSIFIED
SECURITY CLASSIFICATION OF THIS PAGE (When Data Entered)

REPORT DOCUMENTATION PAGE		READ INSTRUCTIONS BEFORE COMPLETING FORM
1. REPORT NUMBER WT-1313 (EX)	2. GOVT ACCESSION NO. AD A995 142	3. RECIPIENT'S CATALOG NUMBER
4. TITLE (and Subtitle) Operation REDWING - Project 2.51 Neutron-Flux Measurements		5. TYPE OF REPORT & PERIOD COVERED DNA
		6. PERFORMING ORG. REPORT NUMBER WT-1313 (EX)
7. AUTHOR(s) C. W. Luke, USA, Project Officer D. L. Rigotti J. W. Kinch, R. Fullwood, D. Anderson		8. CONTRACT OR GRANT NUMBER(s)
9. PERFORMING ORGANIZATION NAME AND ADDRESS U.S. Army Chemical Warfare Laboratories Army Chemical Center, Maryland		10. PROGRAM ELEMENT, PROJECT, TASK AREA & WORK UNIT NUMBERS
11. CONTROLLING OFFICE NAME AND ADDRESS Headquarters Field Command Defense Atomic Support Agency Sandia Base, Albuquerque, New Mexico		12. REPORT DATE September 30, 1959 13. NUMBER OF PAGES
14. MONITORING AGENCY NAME & ADDRESS(if different from Controlling Office)		15. SECURITY CLASS. (of this report) Unclassified 15a. DECLASSIFICATION/DOWNGRADING SCHEDULE

16. DISTRIBUTION STATEMENT (of this Report)

Approved for public release; unlimited distribution.

17. DISTRIBUTION STATEMENT (of the abstract entered in Block 20, if different from Report)

18. SUPPLEMENTARY NOTES

This report has had the classified information removed and has been republished in unclassified form for public release. This work was performed by Kaman Tempo under contract DNA001-79-C-0455 with the close cooperation of the Classification Management Division of the Defense Nuclear Agency.

19. KEY WORDS (Continue on reverse side if necessary and identify by block number)

Operation REDWING
Neutron-Flux Measurements
Neutron Detectors
Neutron Dose Measurements
Gamma-Ray-Dose Measurements

20. ABSTRACT (Continue on reverse side if necessary and identify by block number)

The objectives of this project were to measure the neutron flux and spectrum from the detonation of selected nuclear devices during Operation Redwing. Primary emphasis was placed on measurements during Shot Cherokee, a thermonuclear, high-yield, air burst, and on two shots, Yuma and Kickapoo. Measurements were also made on Shots Blackfoot and Erie . During the operation, permission was granted to make neutron measurements on Shot Osage, a low-yield prototype stockpile warhead unit in a bomb case. Neutron-dose measurements made by chemical and semiconductor dosimeters were compared with the dose calculated by the single-collision theory from the neutron flux and

20. Abstract (Continued)

spectral data. The effect of the presence of different proportions of borax and sulfur on the shielding efficiency of concrete against neutrons was studied during Shot Blackfoot.

Neutron fluxes as a function of distance from ground zero were measured with the following detectors: gold, plutonium, neptunium, uranium, sulfur.

No data were obtained during Shot Cherokee because of the difference between the actual and intended ground zero.

The variation of the neutron flux about the devices fired for Shots Yuma and Kickapoo was energy dependent. The ratios of the neutron flux along a line of 65 degrees to the projection on the ground of the long axis of the device, to that along a line at 0-degrees to this projection for Shot Yuma, were 1.34, 1.91, 1.94, and 1.18 for the plutonium, uranium, sulfur, and gold detectors, respectively. The same ratios between the 85-degree and 0-degree lines for Shot Kickapoo were 1.62, 1.70, 1.62, and 1.22.

Within the range of the measurements made and the accuracy of the threshold detector system there was no variation of the neutron-energy spectrum with increasing distance from the point of detonation.

Any data obtained from an extrapolation of a plot of the neutron flux times slant distance squared versus slant distance to ranges of less than 300 yards may be in error. Theoretical calculations supported by experimental evidence indicate that the relationship is non-linear in this range.

The neutron dose results obtained by using the USAF chemical dosimeters were not consistent with those obtained by the threshold detector technique, ranging from a factor of 1.26 high for Shot Erie to an average factor of 3.54 low for Shot Blackfoot.

The AEC germanium-dosimeter results were lower by factors of 3.46 to 5.38 than those obtained by the threshold-detector technique.

The AEC chemical-dosimeter system may not be used to measure neutron dose in the range of 25,000 to 856,000 rep, due to saturation of the neutron-sensitive dosimeter and difficulties inherent in obtaining accurate readings.

There is little or no increase in the attenuation of fast-neutrons by adding borax or sulfur to concrete. The attenuation of the thermal-neutron flux is increased by adding borax.

The neutron dose was reduced by a factor of approximately four by a concrete box three feet on a side and 6 inches thick fabricated from a mixture containing 1.6 percent borax by weight. The gamma-ray dose, however, was increased by an average factor of 2.75 by similar concrete boxes containing varying amounts of borax and sulfur.

The measured neutron dose per unit yield was higher for all shots than was predicted by TM 23-200. However, only the Yuma, Blackfoot, Kickapoo, and Osage data falls beyond the factor or reliability stated in the manual.

* Per: telecon w/Betty Fox, Chief, DNA Tech Libr'y: Div.: the Classifed References contained herein may remain. 5 Sept.'79
Vic LaChance
DDA-2

**Verified for Extracted Versions.
9 July'80
pfcooper, DTIC/DDA-2

FOREWORD

This report has had classified material removed in order to make the information available on an unclassified, open publication basis, to any interested parties. This effort to declassify this report has been accomplished specifically to support the Department of Defense Nuclear Test Personnel Review (NTPR) Program. The objective is to facilitate studies of the low levels of radiation received by some individuals during the atmospheric nuclear test program by making as much information as possible available to all interested parties.

The material which has been deleted is all currently classified as Restricted Data or Formerly Restricted Data under the provision of the Atomic Energy Act of 1954, (as amended) or is National Security Information.

This report has been reproduced directly from available copies of the original material. The locations from which material has been deleted is generally obvious by the spacings and "holes" in the text. Thus the context of the material deleted is identified to assist the reader in the determination of whether the deleted information is germane to his study.

It is the belief of the individuals who have participated in preparing this report by deleting the classified material and of the Defense Nuclear Agency that the report accurately portrays the contents of the original and that the deleted material is of little or no significance to studies into the amounts or types of radiation received by any individuals during the atmospheric nuclear test program.

SUMMARY OF SHOT DATA, OPERATION REDWING

Shot Name (Unclassified)	Date (PTG)	Time (Approximate)	Location	Type	H&N Coordinates (Actual Ground Zero)	Geographic
						° ′ ″
Lacrosse	5 May	0629	Eniwetok Yvonne	Surface Land	124515 E 106885 N	11 33 29 162 21 18
Cherokee	21 May	0551	Bikini Off Charlie	Air Drop (4320±150 ft) Over Water	96200 ± 100 E 185100 ± 500 N	11 43 50 165 19 46
Zuni	28 May	0556	Bikini Tare	Surface Land Water	110309 E 100154 N	11 29 48 165 22 09
Yuma	28 May	0756	Eniwetok Sally	200-ft Tower	112155 E 130604 N	11 37 24 162 19 13
Erie	31 May	0615	Eniwetok Yvonne	300-ft Tower	127930 E 102060 N	11 32 41 162 21 52
Seminole	6 June	1255	Eniwetok Irene	Surface Land[a]	75237 E 149897 N	11 40 35 162 13 02
Flathead	12 June	0626	Bikini Off Dog	Barge Water	116768 E 164094 N	11 40 22 165 23 13
Blackfoot	12 June	0626	Eniwetok Yvonne	200-ft Tower	126080 E 104435 N	11 33 04 162 21 33
Kickapoo	14 June	1126	Eniwetok Sally	300-ft Tower	114018 E 132295 N	11 37 41 162 19 32
Osage	16 June	1314	Eniwetok Yvonne	Air Drop (680±35 ft) Over Land	126647 ± 50 E 102851 ± 50 N	11 32 48 162 21 39
Inca	22 June	0956	Eniwetok Pearl	200-ft Tower	105300 E 133540 N	11 37 53 162 18 04
Dakota	26 June	0606	Bikini Off Dog	Barge Water	116767 E 164097 N	11 40 22 165 23 13
Mohawk	3 July	0606	Eniwetok Ruby	300-ft Tower	109737 E 132165 N	11 37 39 162 18 49
Apache	9 July	0606	Eniwetok Flora	Barge Water	69227 E 148063 N	11 40 17 162 12 01
Navajo	11 July	0556	Bikini Off Dog	Barge Water	116816 E 160604 N	11 39 48 165 23 14
Tewa	21 July	0546	Bikini Charlie-Dog Reef	Barge Water	99776 E 164476 N	11 40 26 165 20 22
Huron	22 July	0616	Eniwetok Flora	Barge Water	70015 E 148304 N	11 40 19 162 12 09

[a]See ITR-1344 for further details.

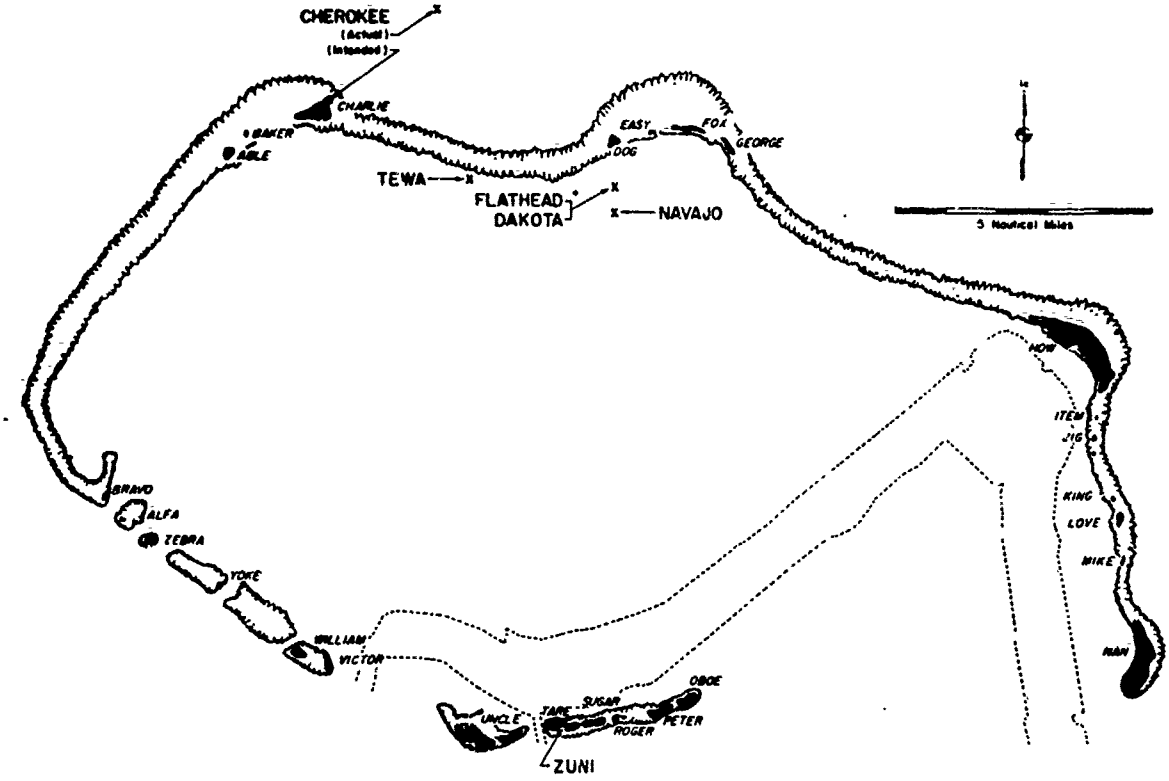

Airukiiji	Oboe	Bokonetokutoku	Alfa	Enitirikku	Uncle	Rochikarai	Love
Airukiraru	Peter	Bokobyaadaa	Able	Eninman	Tare	Romurikku	Fox
Aomoen	George	Bokonejien	Baker	Enyu	Nan	Rukoji	Victor
Arrilkan	Yoke	Bokonfunaku	Item	Ionchebi	Mike	Uorikku	Easy
Bigiren	Roger	Bokororyuru	Bravo	Namu	Charley	Yomyaran	Jig
Bikini	How	Chieerete	William	Ourukaen	Zebra	Yurochi	Dog
		Enisiro	King	Reere	Sugar		

Bikini Atoll. Locations of test detonations during Operation Redwing are indicated by large lettering and arrows. Native island names with corresponding military identifiers are given in the tabulation.

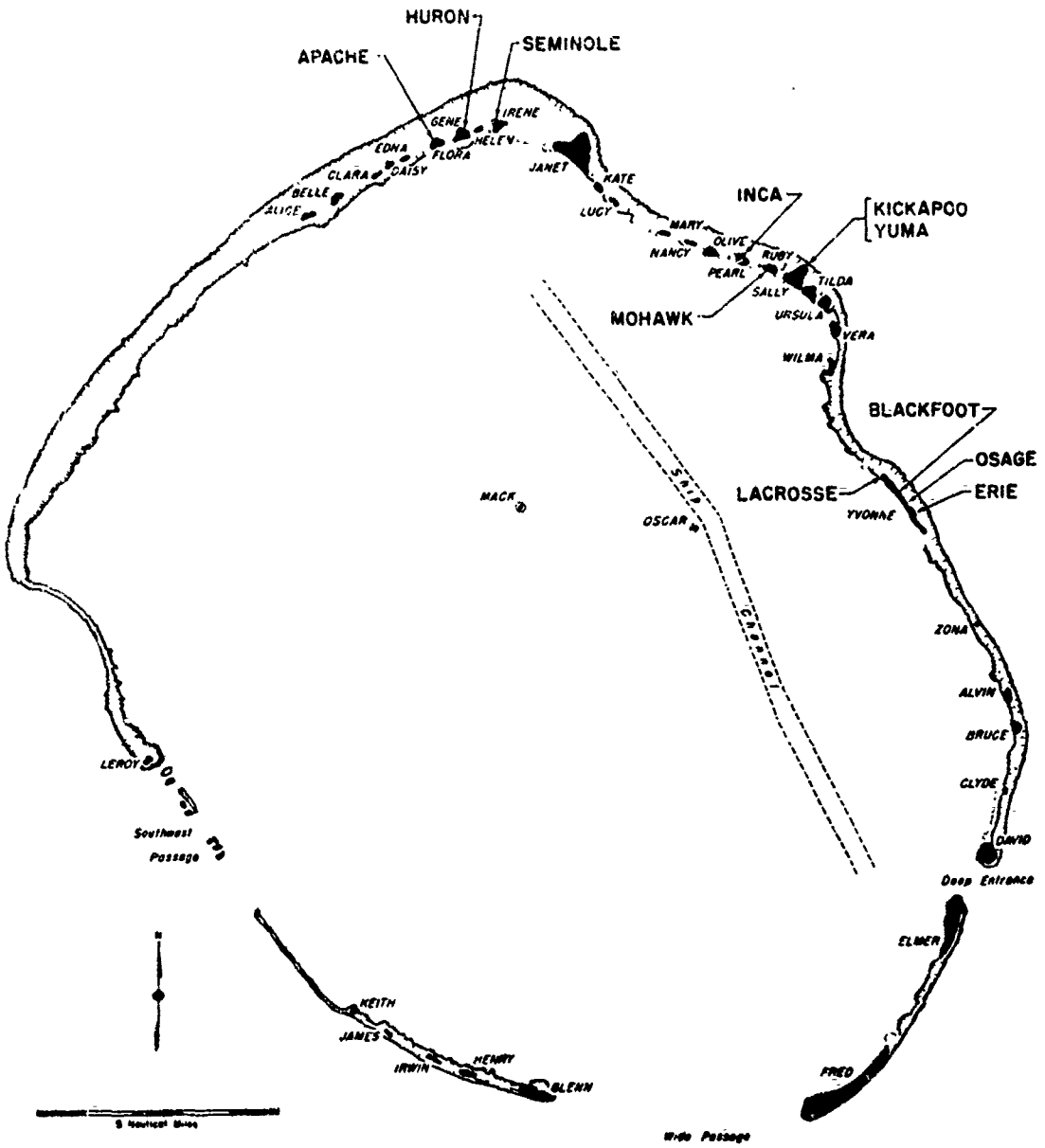

Aaraanbiru	Vera	Chinieero	Alvin	Igurin	Glenn	Ribaion	James
Aitsu	Olive	Chinimi	Clyde	Japtan	David	Rigili	Leroy
Aniyaanii	Bruce	Cochita	Daisy	Kirinian	Lucy	Rojoa	Ursula
Aomon	Sally	Coral Heads	Mack, Oscar	"M"	Zona	Ruchi	Clara
Bijjiri	Tilda	Eberiru	Ruby	Mai	Henry	Rujora	Pearl
Bogairikk	Helen	Elugelab	Flora	Mainn	Kate	Rumit	Yvonne
Bogallua	Alice	Engebi	Janet	Parry	Elmer	Sundildefonso	Edna
Bogon-Bogo	Belle	Eniwetok	Fred	Piiraai	Wilma	Teitelripuechi	Gene
Bogon	Irene	Giriinien	Keith	Pokon	Irwin	Yeiri	Nancy
Bokonaarappu	Mary						

Eniwetok Atoll. Locations of test detonations during Operation Redwing are indicated by large lettering and arrows. Native island names with corresponding military identifiers are given in the tabulation.

ABSTRACT

The objectives of this project were to measure the neutron flux and spectrum from the detonation of selected nuclear devices during Operation Redwing. Primary emphasis was placed on measurements during Shot Cherokee, a thermonuclear, high-yield, air burst, and on two shots, Yuma and Kickapoo. Measurements were also made on Shots Blackfoot and Erie, During the operation. permission was granted to make neutron measurements on Shot Osage, a low-yield prototype stockpile warhead unti in a bomb case. Neutron-dose measurements made by chemical and semiconductor dosimeters were compared with the dose calculated by the single-collision theory from the neutron flux and spectral data. The effect of the presence of different proportions of borax and sulfur on the shielding efficiency of concrete against neutrons was studied during Shot Blackfoot.

Neutron fluxes as a function of distance from ground zero were measured with the following detectors: gold, plutonium, neptunium, uranium, sulfur,

No data were obtained during Shot Cherokee because of the difference between the actual and intended ground zero.

The variation of the neutron flux about the devices fired for Shots Yuma and Kickapoo was energy dependent. The ratios of the neutron flux along a line at 65 degrees to the projection on the ground of the long axis of the device, to that along a line at 0-degrees to this projection for Shot Yuma, were 1.34, 1.91, 1.94, and 1.18 for the plutonium, uranium, sulfur, and gold detectors, respectively. The same ratios between the 85-degree and 0-degree lines for Shot Kickapoo were 1.62, 1.70, 1.62, and 1.22.

Within the range of the measurements made and the accuracy of the threshold detector system there was no variation of the neutron-energy spectrum with increasing distance from the point of detonation.

Any data obtained from an extrapolation of a plot of the neutron flux times slant distance squared versus slant distance to ranges of less than 300 yards may be in error. Theoretical calculations supported by experimental evidence indicate that the relationship is non-linear in this range.

The neutron dose results obtained by using the USAF chemical dosimeters were not consistent with those obtained by the threshold detector technique, ranging from a factor of 1.26 high for Shot Erie to an average factor of 3.54 low for Shot Blackfoot.

The AEC germanium-dosimeter results were lower by factors of 3.46 to 5.38 than those obtained by the threshold-detector technique.

The AEC chemical-dosimeter system may not be used to measure neutron dose in the range of 25,000 to 856,000 rep, due to saturation of the neutron-sensitive dosimeter and difficulties inherent in obtaining accurate readings.

There is little or no increase in the attenuation of fast-neutrons by adding borax or sulfur to concrete. The attenuation of the thermal-neutron flux is increased by adding borax.

The neutron dose was reduced by a factor of approximately four by a concrete box three feet on a side and 6 inches thick fabricated from a mixture containing 1.6 percent borax by weight. The gamma-ray dose, however, was increasad by an average factor of 2.75 by similar concrete boxes containing varying amounts of borax and sulfur.

The measured neutron dose per unit yield was higher for all shots than was predicted by TM 23-200. However, only the Yuma, Blackfoot, Kickapoo, and Osage data falls beyond the factor or reliability stated in the manual.

FOREWORD

This report presents the final results of one of the projects participating in the military-effect programs of Operation Redwing. Overall information about this and the other military-effect projects can be obtained from WT-1344, the "Summary Report of the Commander, Task Unit 3." This technical summary includes: (1) tables listing each detonation with its yield, type, environment, meteorological conditions, etc.; (2) maps showing shot locations; (3) discussions of results by programs; (4) summaries of objectives, procedures, results, etc., for all projects; and (5) a listing of project reports for the military-effect programs.

PREFACE

The authors wish to express their appreciation for the efforts of all personnel who were assigned to the project. The efforts of these individuals were instrumental in the satisfactory completion of the project.

The authors wish to acknowledge Wendell Biggers, Los Alamos Scientific Laboratory and G.S. Hurst, Oak Ridge National Laboratory for invaluable aid and service rendered during calibration of equipment; the Department of Radiobiology, School of Aviation Medicine, USAF, particularly for the chemical dosimeter measurements obtained in the field by 1st Lt. Sanford C. Sigoloff, USAF; and Drs. Dunham, Corsbie, and Butenhoff, for making available to this study the AEC dosimeter systems described in this report; Drs. Taplin and Cassen, UCLA Atomic Energy Project, for their production and evaluation of the AEC dosimeter systems.

CONTENTS

TABLES

Chapter 1
INTRODUCTION

1.1 OBJECTIVES

The objectives of Project 2.51 in Operation Redwing were to: (1) measure the neutron flux from selected nuclear devices as a function of distance from their respective points of detonation, and evaluate the angular distribution of neutron flux of [redacted] devices; (2) investigate the energy spectrum of the neutron flux produced by these devices by means of a system of threshold detectors; (3) compare the threshold-detector method of determining the dose in rep with chemical and semiconductor dosimeter methods; (4) measure the relative attenuation of neutron flux by various concrete mixtures containing borax and sulfur; and (5) compare the results obtained with those from previous operations.

1.2 PURPOSE

The primary purpose of this study was to document the neutron flux from various nuclear devices including an air-dropped megaton-range device, and to investigate the neutron spatial distribution from the detonation of [redacted] devices. The detonation of a low-yield [redacted] device provided an opportunity to study the variation of the neutron spectrum with distance for this type of device. This low-yield, [redacted] shot also allowed the testing of a suggestion advanced by the Corps of Engineers that the neutron attenuation by the concrete used in military construction might be increased by the incorporation of borax or sulfur in the mix. This study also afforded the opportunity to field test recently developed neutron dosimeters.

1.3 BACKGROUND

1.3.1 General. There are two general reasons for measuring the neutron flux of a nuclear device: (1) the evaluation of the operation of the device, and (2) the evaluation of the effects of the neutrons on matter external to the device. The establishment of the number and energy of the neutrons and their spatial distribution is of basic importance to the assessment of the effects of the neutrons from a device. Measurements of this nature are called neutron-flux measurements and have been made by the Department of Defense (DOD) agencies in the past.

In order to convert the neutron-flux measurements into terms which can be interpreted as the effect of neutrons on tissue or other materials, a relationship must be established between the neutron flux and the energy transfer to these materials. The measurements describing this energy transfer are called neutron-dose measurements. A discussion of the relationship between neutron flux and neutron-dose measurements will be given later.

1.3.2 Neutron-Flux Measurements. Two basic types of neutron-flux measurements have been made during past operations. Measurements were made in good geometry, or where the neutron beam was collimated during Operation Greenhouse (Reference 1) and Operation Upshot-Knothole

(Reference 2). The second type of flux measurements that have been made are those made in poor geometry, or where the uncollimated beam was measured. This type of measurement was made during nearly all past operations.

Neutron measurements have been made over a wide range of yields. As yet, no successful measurements have been made for a megaton-range device. Attempts to measure the neutron flux from the multimegaton shots of Operation Castle (Reference 3) failed, due to adverse operating conditions. These conditions were: extreme damage at close-in stations due to high overpressures, lack of sufficient land on which to place stations, long recovery times required; excessive contamination of the counting area after the first shot; and contamination of the samples, believed to be caused by contaminated water leaking into the sample holders.

Previous operations (Reference 4) have indicated that the neutron flux from an asymmetric device is approximately 30 percent higher along a line perpendicular to the long axis of the device compared to that parallel to the long axis. Since this type of device has a high neutron-to-gamma ratio, it is of interest to establish the variation of the neutron flux with the geometry of this type device.

In the work done by the Civil Effects Group, Project 39.7, during Operation Teapot (Reference 5), it was shown that, [redacted] there is no apparent modification of the neutron spectrum at increasing distances from ground zero. This is evidenced by the fact that the plots of flux times slant range squared versus slant range for the various threshold detectors are parallel within the statistical variation of the data. This fact may have a considerable effect in simplifying the documentation of the neutron fluxes from future devices, since the number of detectors required could be reduced considerably.

1.3.3 Neutron Detectors. Neutron measurements using the threshold detector technique have been made on nearly all past operations (References 1 through 12). The conditions under which these neutron measurements were made necessitated the development of a measuring system which was rugged and insensitive to outside factors (such as gamma-ray fields and high thermal fluxes) and which allowed the data to be collected at relatively long periods of time after the short initiating event had taken place. The neutron-flux measurements made prior to Operation Teapot consisted mainly of measurements of thermal neutrons by the use of gold as a detector, and of neutrons above 3 Mev using sulfur as a detector.

During Operation Upshot-Knothole (Shot 10), a high-neutron flux was realized from a [redacted] necessitating the investigation of a neutron-produced dose, which could be a major casualty-producing effect of this type of weapon.

As a result of this added emphasis on neutrons, several attempts were made to develop detectors for neutrons in the biologically-interesting region between thermal and 3-Mev neutrons. The culmination of these attempts was the development of the fission-threshold detectors by G. S. Hurst of the Oak Ridge National Laboratory (ORNL). This system of detectors consists of gold plus cadmium-shielded gold, boron-shielded plutonium^{239}, neptunium^{237}, uranium^{238}, and sulfur. The gold is used to measure the total number of thermal neutrons, while the remaining detectors measure the number of neutrons above 10 kev, 0.63 Mev, 1.5 Mev, and 3 Mev, respectively. A discussion of the reaction and experimental techniques used for each of the above detectors is given in Chapter 2.

The development of thermonuclear [redacted] weapons brought about an interest in the 14.2 Mev neutrons, with a resultant development and use of iodine [redacted] detectors for these high-energy neutrons.

By successive subtraction of the integrated fluxes of the various threshold detectors above 10 kev, it is possible to obtain an indication of the neutron spectrum in the region from 10 kev to 14 Mev.

1.3.4 Neutron Dose Measurements. A first-collision tissue-dose for fast neutrons has been reported (Reference 13). This curve is based on the assumption that the entire dose is caused by the first collision of neutrons. The dose per neutron/cm^2 varies with energy as the quantity $E\Sigma_i\sigma_i f_i N_i$ where σ_i is the scattering cross section of the i^{th} kind of atom, f_i is the average fractional loss of energy per collision of the neutron with the i^{th} kind of atom and N_i is the number per unit mass of the i^{th} kind of atom. The summation is to be taken for hydrogen, oxygen, carbon, and nitrogen. By assuming the composition of tissue to be 10 percent hydrogen, 73 percent oxygen, 12 percent carbon and 4 percent nitrogen, a relationship between dose per neutron/cm^2 and neutron energy was established from the definition of the rep unit and the fact that the dose is proportional to $\Sigma\Sigma_i\sigma_i f_i N_i$. Figure 1.1 is a plot of dose for one neutron per square centimeter as a function of energy (Reference 14).

By taking the dose per neutron/cm^2 at the average energy between the effective threshold of the above detector system, the following equation was determined (Reference 14):

$$D = [0.029\ N_T + 1.0\,(N_{Pu} - N_{Np}) + 2.5\,(N_{Np} - N_U) + 3.2\,(N_U - N_S) + 3.0\ N_S]\ 10^{-9} \quad (1.1)$$

Where: D = the dose in rep

N_T = the thermal flux

N_{Pu}, N_{Np}, N_U, and N_S = the number of neutrons per square centimeter above the thresholds for Pu, Np, U, and S, respectively.

Agreement between dose measurements made with this system of detectors and the Hurst proportional-neutron counter using the ORNL cyclotron, the ORNL tower-shielding facility, and the LASL Godiva assembly as neutron sources was very good. In the case of a thermonuclear device, Equation 1.1 is changed to include an additional term due to the presence of a relatively large amount of 14.2 Mev neutrons yielded by (d, t) reaction. As has been previously mentioned, the neutrons having energies greater than 12 Mev are measured, utilizing detectors. Therefore, Equation 1.1 would be written:

$$D = [0.029\ N_T + 1.0\,(N_{Pu} - N_{Np}) + 2.5\,(N_{Np} - N_U) + 3.2\,(N_U - N_S) + 5.3\,(N_S - N_{Zr}) + 6.5\,(N_{Zr})]\ 10^{-9} \quad (1.2)$$

Where the coefficient for the $(N_S - N_{Zr})$ term is determined in the aforementioned manner, since the neutrons above the 12-Mev threshold are within a very small energy range around this point.

Preliminary results were obtained using the above system during Operation Castle (Reference 3). The complete system was used successfully during Operation Teapot by the Civil Defense Test Group, Project 39.7 (Reference 5), and Naval Research Laboratory (NRL), Project 2.2 (Reference 4).

1.3.5 Other Neutron Dosimeters. During Operation Teapot, chemical dosimeters were, for the first time, successfully used to measure the neutron dose (Reference 5). As indicated in the reference, two general classes of chemical dosimeters were used for this purpose. The two classes were the fast-neutron insensitive anhydrous chloroform and tetrachloroethylene systems, and the neutron-and-gamma-sensitive halogenated-hydrocarbon dye water-equivalent system. Further details of these systems are given in Chapter 2 of this report.

Agreement between the chemical dosimeter method and the fission-foil method of measuring

neutron dose was within 30 percent during Operation Teapot. Recent calibrations accomplished by Langham, Harris, Hurst, Sayeg, and Sigoloff utilizing Godiva I at the Los Alamos Scientific Laboratory indicate agreement of ± 10 percent between these systems.

Germanium is a semiconductor whose conductance, on exposure to fast neutrons, changes proportionally with the neutron flux. When a germanium crystal is irradiated with fast neutrons, the crystal lattice is disrupted by the resultant recoils of the germanium atoms. The defects in the lattice structure act as traps for the electrons in the Fermi levels. The unoccupied Fermi levels, or holes, act as though they were positive electrons, changing the conductivity of the crystals. The resultant change in the conductivity is proportional to the number of neutrons

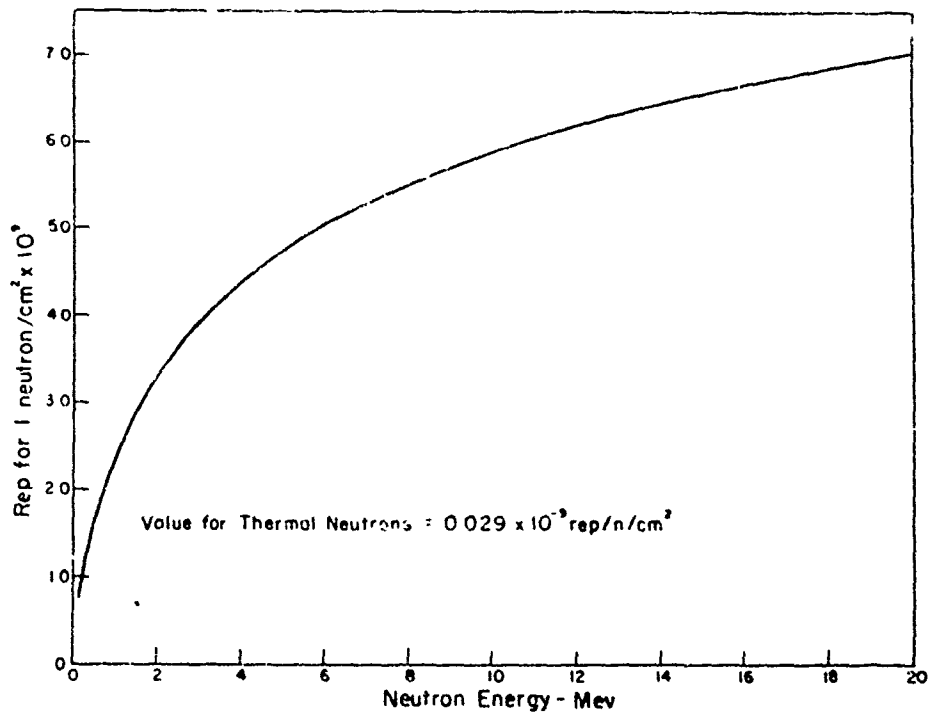

Figure 1.1 Neutron dose as a function of energy.

passing through the crystal. The sensitivity to neutrons of 0.5 Mev or less is low for plain-germanium crystals. By adding small amounts of gold to the crystal, the sensitivity toward the lower-energy neutrons can be increased. There has been little or no sensitivity to gamma rays found in the germanium crystals when exposed to gamma rays of energies comparable to those found in a fission spectrum. Cassen and others, (Reference 15) concluded from results of their measurements during Operation Upshot-Knothole that suitably-calibrated germanium could be used as a simple fast-neutron dosimeter. The results of measurements made during Operation Castle (Reference 3) were inconclusive. The results of measurements made during Operation Teapot (Reference 16) were published in terms of relative values. No conclusions were made from the preliminary data.

1.4 THEORY

The fission process is well known and needs no further discussion here. It suffices to say

that a certain fraction of the total number of neutrons produced is required to maintain the fission process. The fraction of the original number of neutrons produced which escapes the fission process must pass through the material of the device; and in passing through this material, a portion of these neutrons can be absorbed or scattered by the material. In general, the latter process results in a degradation of the energy of the neutrons and a change of their angular distribution, while the former completely removes the neutrons from the system. As the neutrons pass into the air, the absorption and scattering processes continue. Both the absorption and scattering processes are functions of the energy of the neutrons and of the material through which they pass.

As a result of these processes, the number of neutrons which reach a given volume in space outside a nuclear device will consist of those original neutrons produced by the source which escape the absorption and scattering process plus an additional number of neutrons which have been scattered. Any quantitative consideration of this problem would, of course, have to consider the reduction of the number of neutrons due to the spherical geometry of the problem. A mathematical formulation of this problem is given by the Boltzmann transport equation (Appendix).

Solutions of the transport equation for several monoenergetic point sources in air have been calculated. Through a series of operative techniques, these solutions to the transport equation can be compared to the measurements made in the field. A discussion of the technique used, and comparison with past field measurements, is given in the Appendix to this report.

The solution of the complete transport equation is an extremely difficult problem. It is beyond the scope of this report to go into the many other approximate methods for the solution. At the present time, it would appear that a combination of a Monte-Carlo technique combined with moment-method solutions of the transport equations may be the most-valuable approach. For the conditions under which the neutron-flux measurements have been made, there are, as yet, no solutions to the transport equation.

In the past, the fast-neutron data have been presented in graphical form on a semi-logarithmic graph. The neutron flux times the square of the slant range has been plotted against the slant range. A resultant straight line thus suggests that the neutrons (nvt) as a function of slant range (r) can be described by the following equation:

$$nvt = \frac{A}{r^2} \exp(-kr) \tag{1.3}$$

Where A and k = constants

This equation has the same form as that which can be derived for the attenuation of a monoenergetic neutron beam passing through matter assuming only absorption, and that scattering of the neutrons will remove them from the measured neutron beam. This equation is:

$$nvt = \frac{I_0}{4\pi^2} \exp(-\Sigma r) \tag{1.4}$$

where I_0 is the total number of neutrons emitted by the source and nvt is the number of neutrons which succeed in passing through a unit area at a distance r of the material. The total microscopic cross section of the material is Σ. The $4\pi r^2$ takes into consideration of the spatial divergence of the spherical geometry.

At a given energy, the mean free path λ is equal to $1/\Sigma$. From this analogy, the slope of the measured data obtained for fluxes with arbitrary spectra has been called a measure of the mean free path. As shown by results of the solution of the transport equation as given in the

Appendix, the theoretical curve does approach this straight-line relation when plotted on a semi-log graph. It is indicated in the Appendix that, based on the theoretical solution, a straight-line extrapolation of the data beyond the measured data may be erroneous.

In the past, the thermal-neutron flux has been presented graphically in two ways. During Operation Ranger (Reference 10), it was presented in the same manner as the fast neutrons. In the more recent references, the thermal neutron flux times the slant range has been plotted against the slant range. The latter plot is based on predictions for the penetration of thermal neutrons in matter based on diffusion theory which gives a $\frac{1}{r}$ dependence. Diffusion theory does not apply in this case. There appears to be no a priori reason for the spatial dependence of thermal neutrons to differ radically from that of neutrons of high energy (cf, discussion in Reference 23). The thermal-neutron data in this report will be presented in the same manner as the fast-neutron data.

Chapter 2
PROCEDURE

2.1 PARTICIPATION

Project 2.51 participated in six shots during Operation Redwing. The shot participation was dictated by two major factors: the type of device to be detonated, and the land area available for instrumentation. Pertinent information relative to these six shots may be found in Table 2.1.

2.2 STATION PLACEMENT

The limited land area and crowded conditions on the shot sites restricted the choice of positions for Project 2.51 stations. The location of the stations, distances from the point of detonation, and the type of detectors for the six shots in which this project participated are given in Table 2.2. Figures 2.1, 2.2, and 2.4 are diagrams of the station locations for Shot Cherokee; Shots Blackfoot, Erie, and Osage; and Shots Yuma and Kickapoo, respectively. Complete coverage of all stations with plutonium, uranium, and neptunium samples was not possible because of an inadequate supply of these detectors, and late changes in shot schedules, which prevented the reuse of detectors on successive shots.

2.3 STATION DESIGN

The stations for Shot Cherokee consisted of concrete slabs to which were bolted steel plates $1\frac{1}{2}$ feet by $5\frac{1}{2}$ feet by 1-inch (Figure 2.5). The concrete slabs at the land stations were 12 feet long by 6 feet wide by 6 feet deep. The steel plates were oriented so that they would be perpendicular to a line from the station to the intended point of burst. In order to facilitate recovery, the detectors were mounted on the steel plates by specially designed quick-disconnect clamps.

Three instrument lines were required to determine the variation of the neutron flux with angle about the asymmetric devices detonated in Shots Yuma and Kickapoo. One line extended along the projection on the ground of the long axis of the device, the second line extended at 45 degrees to this line, and a third line extended at 64 degrees for Shot Yuma and 85 degrees for Shot Kickapoo to the projection of the long axis of the device. It was desired that the third line be placed at 90 degrees to the long axis of the device; however, a permanent structure housing diagnostic measuring equipment along this line precluded the possibility of constructing an instrument line in this direction. Past experiments (Reference 4) had indicated that the variation of the neutron flux with angle was not great beyond 45 degrees from the long axis; therefore, an angle less than 90 degrees was chosen in order to have a continuous straight exposure line. The instrument lines used for Shot Yuma consisted of 1-inch steel cables laid along the ground. At 100-yard intervals from ground zero the field detector holders were clamped to the cable. The cable and holders at each of the 100-yard stations were raised off the ground by sandbags or 3-foot-high wooden horses, in order to insure a clear line of sight between the detector and device to be detonated. For Shot Kickapoo it was required that one of the lines extend along the seaward reef of the island. For this line, each 100-yard station consisted of 3-inch pipe driven into the reef. Welded to the top of this pipe was a $\frac{3}{4}$-inch rod, to which the standard field detector holders were clamped.

For Shot Blackfoot the instrument line established by Project 12.1 was used. This line was

also along the seaward reef and consisted of the same type of stations that were used during Shot Kickapoo.

For Shot Erie two stations were instrumented at the request of Project 19.1. A complete set of threshold detectors was placed at each of these stations. In addition, sulfur and chemical dosimeters were placed along the Project 12.1 instrument line. This line consisted of stake stations of the same design as those used for Shots Blackfoot and Kickapoo. Participation in Shot Osage depended upon whether or not the device was to be detonated over land or water. The decision to participate came at a late date and consequently, hasty arrangements for stations had to be made. The stations consisted of $\frac{3}{4}$-inch steel reinforcing rods to which the sample holders were clamped.

2.4 NEUTRON SHIELDING BY SPECIAL CONCRETES

Specially prepared concrete mixes, containing different proportions of sulfur and borax, were used to construct five-sided boxes with 6-inch-thick walls. The boxes, which were 3-foot cubes, were emplaced with their open side set 6-inches below the ground level along an arc approximately 750 feet from the point of detonation of Shot Blackfoot (Figure 2.2), and were instrumented both inside and outside with neutron detectors, neutron dosimeters, and gamma-ray dosimeters (Figure 2.3).

The compositions of the concrete boxes were: Box 1, ordinary reinforced concrete, no admixture, approximate weight of concrete 2,500 pounds; Box 2, which was fabricated by Beall Construction Company, Sarasota, Florida, utilized a special concrete without reinforcing, trade name (Thermo Con), no admixture, approximate weight of concrete 1,500 pounds; Box 3, reinforced concrete with 20 pounds of borax added to the water before mixing, approximate weight of concrete 2,500 pounds; Box 4, reinforced concrete with 40 pounds of borax added to the water before mixing, approximate weight of concrete 2,500 pounds; Box 5, reinforced concrete with 60 pounds of borax added to the water before mixing, approximate weight of concrete 2,500 pounds; Box 6, reinforced concrete with 15 pounds of sulfur added to the fine aggregate before mixing, approximate weight of concrete 2,500 pounds.

2.5 METHODS OF MEASUREMENT

Counting of the exposed threshold detectors was accomplished at the two mobile laboratories

TABLE 2.2 PROJECT 2.51 DETECTOR STATIONS

Station	Site	Distance from Ground Zero	Azimuth from Ground Zero	Shot	Description
		ft			
250.01	Charlie	80	270°	Cherokee	Au, S, 2 sets of 3 fission detectors, chemical and germanium dosimeters
250.02	Charlie	1,250	270°	Cherokee	Au, S, 2 sets of 3 fission detectors, chemical and germanium dosimeters
250 03	Charlie	2,500	270°	Cherokee	Au, S, 2 sets of 3 fission detectors, chemical and germanium dosimeters
251 01	Reef E of Charlie	7,500	135°	Cherokee	Au, S, 2 sets of 3 fission detectors, chemical and germanium dosimeters
252.01	Yvonne	348	337° 28′ 33″	Blackfoot	Au, S, CD and GD, (chemical and germanium dosimeters)
252.02	Yvonne	442	337° 28′ 33″	Blackfoot	Au, S, CD, GD
252.03	Yvonne	627	337° 28′ 33″	Blackfoot	Au, S, CD, GD
252.04	Yvonne	961	337° 28′ 33″	Blackfoot	Au, S, Pu, U, CD, GD
252.05	Yvonne	1,295	337° 28′ 33″	Blackfoot	Au, S, Pu, U, CD, GD
252.06	Yvonne	1,626	337° 28′ 33″	Blackfoot	Au, S, CD, GD
252.07	Yvonne	1,957	337° 29′ 33″	Blackfoot	Au, S, Pu, U, CD, GD
252.08	Yvonne	2,287	337° 28′ 33″	Blackfoot	Au, S, CD, GD
252.09	Yvonne	2,616	337° 28′ 33″	Blackfoot	Au, S, Pu, U, CD, GD
252.10	Yvonne	2,945	337° 28′ 33″	Blackfoot	Au, S, CD, GD
252.11	Yvonne	3,274	337° 28′ 33″	Blackfoot	Au, S, CD, GD
255 01	Yvonne	750	315°	Blackfoot	Au, S, Pu, U CD
253.01	Sally	300	110° 28′ 26″	Yuma	Au, S, Pu, U, CD, GD
253.02	Sally	600	110° 28′ 26″	Yuma	Au, S, Pu, U, Np, CD, GD
253 03	Sally	900	110° 28′ 26″	Yuma	Au, S, Pu, U, CD, GD
253.04	Sally	1,200	110° 28′ 26″	Yuma	Au, S, Pu, U, CD, GD
253 05	Sally	1,500	110° 28′ 26″	Yuma	Au, S, Pu, U, CD, GD
253.06	Sally	1,800	110° 28′ 26″	Yuma	Au, S, Pu, U, CD, GD
253.08	Sally	300	67° 28′ 26″	Yuma	Au, S, Pu, U, CD, GD
253.09	Sally	600	67° 28′ 26″	Yuma	Au, S, Pu, U, CD, GD
253 10	Sally	900	67° 28′ 26″	Yuma	Au, S, Pu, U, CD, GD
253 11	Sally	1,200	67° 28′ 26″	Yuma	Au, S, Pu, CD, GD
253 12	Sally	1,500	67° 28′ 26″	Yuma	Au, S, Pu, U, CD, GD
253.13	Sally	1,800	67° 28′ 26″	Yuma	Au, S, CD, GD
253.15	Sally	300	46° 38′ 26″	Yuma	Au, S, Pu, U, Np, CD, GD
253.16	Sally	600	46° 38′ 26″	Yuma	Au, S, Pu, U, CD, GD
253.17	Sally	900	46° 38′ 26″	Yuma	Au, S, Pu, U, CD, GD
253.18	Sally	1,200	46° 38′ 26″	Yuma	Au, S, Pu, U, CD, GD
253.19	Sally	1,500	46° 38′ 26″	Yuma	Au, S, Pu, U, CD, GD
253 20	Sally	1,800	46° 38′ 26″	Yuma	Au, S, Pu, CD, GD
253.21	Sally	2,100	46° 38′ 26″	Yuma	Au, S, Pu, U, CD, GD
253.22	Sally	300	236° 06′ 44″	Kickapoo	Au, S, CD, GD
253.23	Sally	600	236° 06′ 44″	Kickapoo	Au, S, Pu, U, CD, GD
253.24	Sally	900	236° 06′ 44″	Kickapoo	Au, S, CD, GD

TABLE 2.2 CONTINUED

Station	Site	Distance from Ground Zero	Azimuth from Ground Zero	Shot	Description
		ft			
253.25	Sally	1,200	236° 06′ 44″	Kickapoo	Au, S, Pu, U, Np, CD, GD
253.26	Sally	1,500	236° 06′ 44″	Kickapoo	Au, S, CD, GD
253.27	Sally	1,800	236° 06′ 44″	Kickapoo	Au, S, Pu, U, Np, CD, GD
253.28	Sally	2,100	236° 06′ 44″	Kickapoo	Au, S, CD, GD
253.29	Sally	2,400	236° 06′ 44″	Kickapoo	Au, S, Pu, U, CD, GD
253.32	Sally	300	212° 22′ 15″	Kickapoo	Au, S, CD, GD
253.33	Sally	600	204° 52′ 15″	Kickapoo	Au, S, Pu, U, CD, GD
253.34	Sally	900	195° 52′ 15″	Kickapoo	Au, S, CD, GD
253.35	Sally	1,200	195° 52′ 15″	Kickapoo	Au, S, Pu, U, CD, GD
253.36	Sally	1,500	195° 52′ 15″	Kickapoo	Au, S, CD, GD
253.37	Sally	1,800	195° 52′ 15″	Kickapoo	Au, S, Pu, U, CD, GD
253.38	Sally	2,100	195° 52′ 15″	Kickapoo	Au, S, CD, GD
253.39	Sally	2,400	195° 52′ 15″	Kickapoo	Au, S, CD, GD
253.40	Sally	2,700	195° 52′ 15″	Kickapoo	Au, S, CD, GD
253.42	Sally	300	150° 52′ 15″	Kickapoo	Au, S, CD, GD
253.43	Sally	600	150° 52′ 15″	Kickapoo	Au, S, Pu, U, CD, GD
253.44	Sally	900	150° 52′ 15″	Kickapoo	Au, S, CD, GD
253.45	Sally	1,200	150° 52′ 15″	Kickapoo	Au, S, Pu, U, Np, CD, GD
253.46	Sally	1,500	150° 52′ 15″	Kickapoo	Station Missing
253.47	Sally	1,800	150° 52′ 15″	Kickapoo	Au, S, CD, GD
253.48	Sally	2,100	150° 52′ 15″	Kickapoo	Au, S, Pu, U, CD, GD
253.49	Sally	2,400	150° 52′ 15″	Kickapoo	Au, S, CD, GD
253.50	Sally	2,700	150° 52′ 15″	Kickapoo	Au, S, Pu, U, CD, GD
253.51	Sally	3,000	150° 52′ 15″	Kickapoo	Au, S, CD, GD
1210.01	Yvonne	200.6	154° 47′ 43″	Erie	Chemical dosimeters, S, Au
1210.03	Yvonne	934.0	154° 47′ 43″	Erie	Chemical dosimeters, S, Au
1210.05	Yvonne	1,601.9	154° 47′ 43″	Erie	Chemical dosimeters, S, Au
1210.07	Yvonne	2,276.9	154° 47′ 43″	Erie	Chemical dosimeters, S, Au
1210.09	Yvonne	2,937.3	154° 47′ 43″	Erie	Chemical dosimeters, S, Au
1911.01	Yvonne	935	192° 33′ 00″	Erie	Au, S, Pu, U, Np
1911.02	Yvonne	1,290	176° 11′ 00″	Erie	Au, S, Pu, U, Np
1 N	Yvonne	155	NW	Osage	Au, S, Pu, U
1 S	Yvonne	155	SE	Osage	Au, S, Pu, U, Np
2 S	Yvonne	455	SE	Osage	Au, S, Pu, U, Np
3 S	Yvonne	755	SE	Osage	Au, S, Pu, U, Np
4 S	Yvonne	1,055	SE	Osage	Au, S, Pu, U, Np
5 S	Yvonne	1,355	SE	Osage	Au, S, Pu, U

set up on Site Elmer. All counting was done by Project 2.51 personnel. The general procedure followed for each of the detectors was to establish the counting rate that existed at completion of irradiation or at some specific time after irradiation and, by means of calibration numbers, convert these data to integrated neutron flux.

2.5.1 Gold-Neutron Detectors. The Au^{197} (n, γ) Au^{198} reaction was used for the gold detectors. The reaction is characterized by a 64.8-hour half life with the Au^{198} decaying to stable Hg^{198} by the emission of a 0.97 Mev beta particle followed by a 0.411-Mev gamma ray. There are no observable interfering activities.

The cadmium-difference technique was used for measuring the thermal-neutron flux with gold. The cadmium cross section for neutrons drops rapidly from a high of 2,500 barns at 0.04 ev to

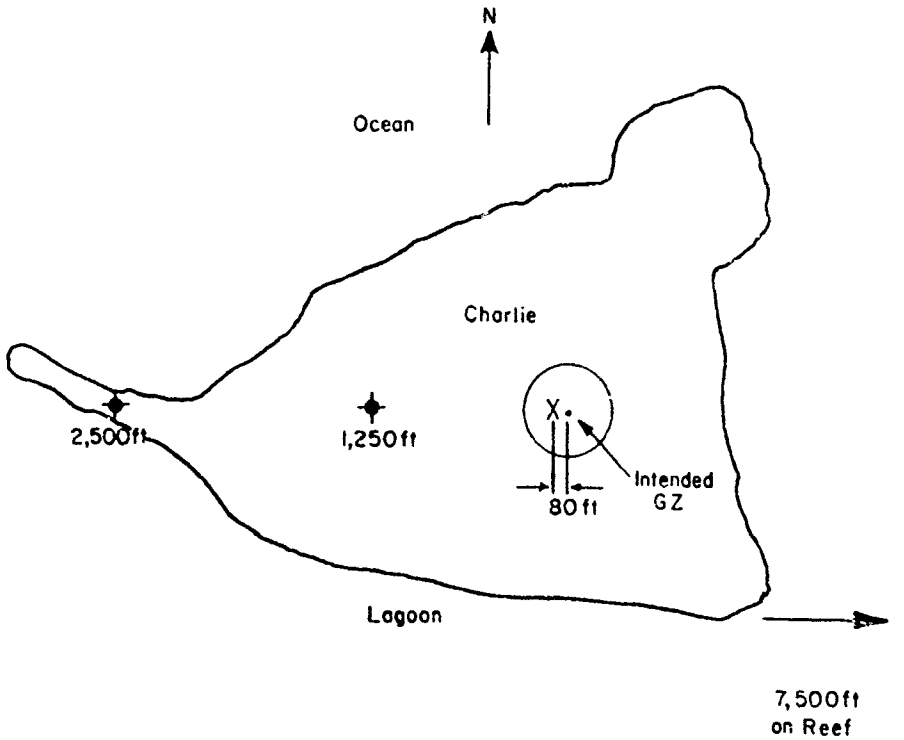

Figure 2.1 Station locations for Shot Cherokee.

23 barns at 1.0 ev (Reference 17). This rapid change in cross section is known as the cadmium cutoff. Gold, on the other hand, has a cross section which has a 1/v slope in the thermal region, with a high resonance peak of 10,000 barns at 4.8 electron volts. The major portion of the activity produced in gold by bombardment with neutrons above thermal energies will be due to this resonance. Therefore, when two gold foils are exposed, one shielded with cadmium and the other bare, the difference in the resultant activities of the two foils eliminates the gold resonance peak and is proportional to the thermal-neutron flux.

One-half-inch-diameter, 10-mil-thick gold foils were placed in field holders. The field holders consisted of two $\frac{1}{4}$-inch steel plates bolted together. Cavities were milled in one of the plates which would accept one bare foil and one cadmium-shielded foil. The cadmium shield was 0.045-inch thick. A mounting web was welded to one of the plates to enable the assembled detector to be attached to the cable or pipe station by U bolts.

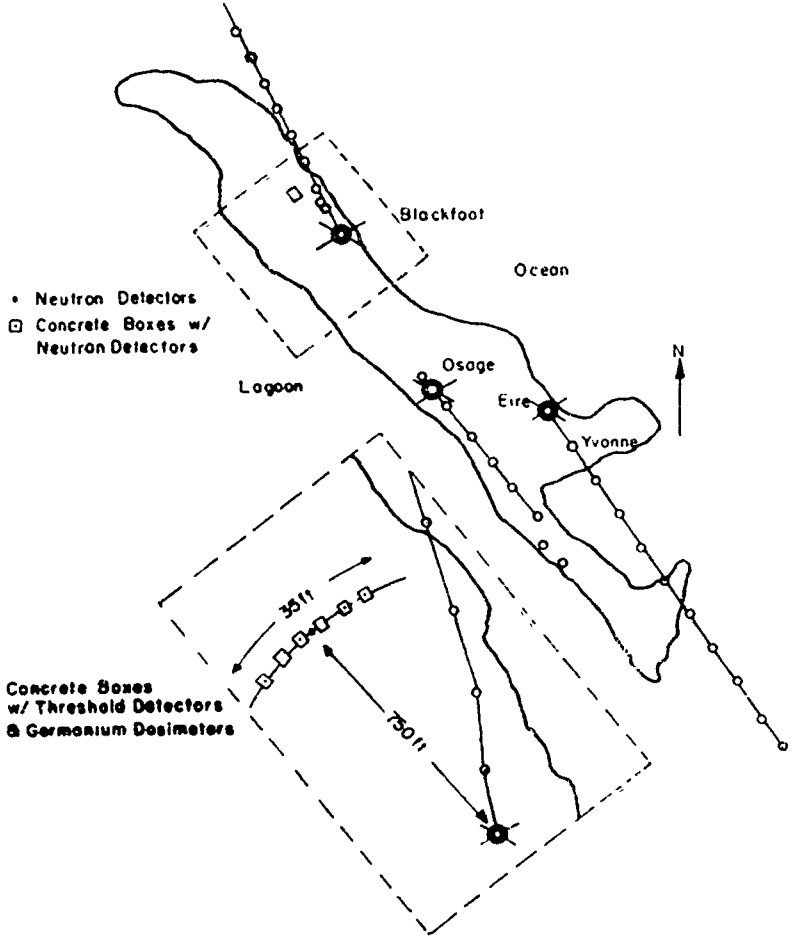

Figure 2.2 Station locations for Shots Blackfoot, Erie, and Osage.

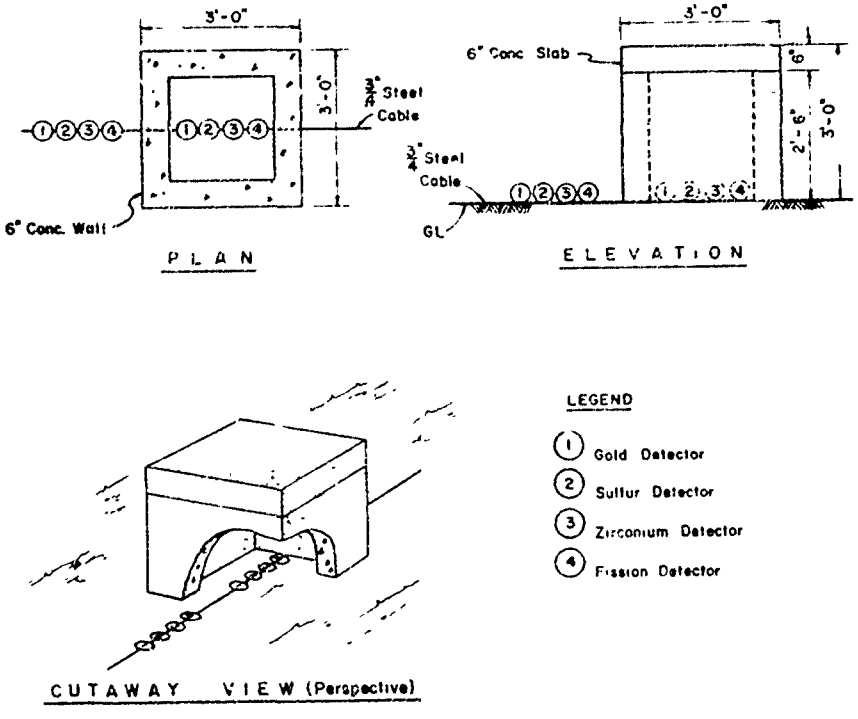

Figure 2.3 Typical concrete boxes instrumented with neutron detectors.

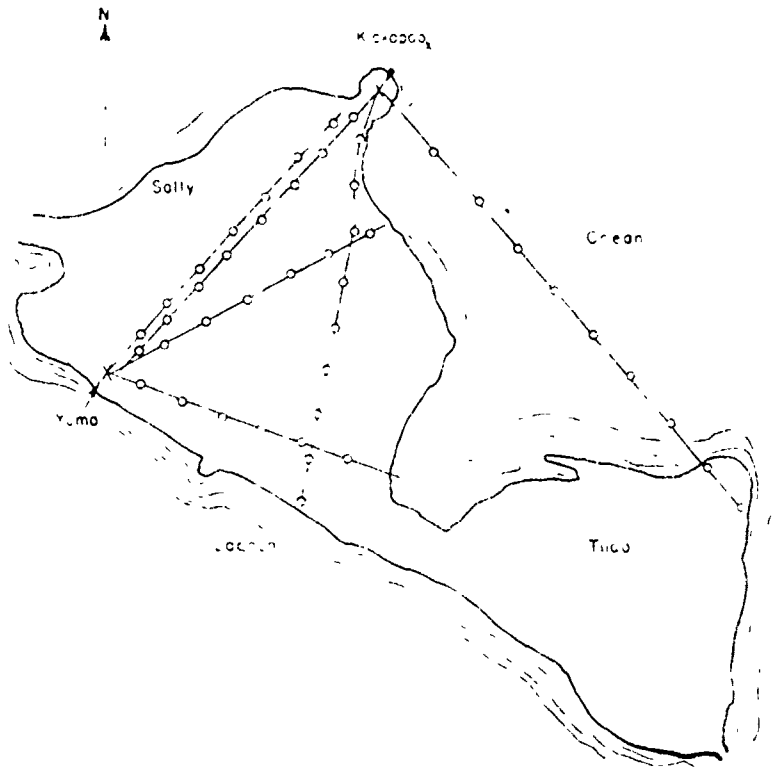

Figure 2.4 Station locations for Shots Yuma and Kickapoo.

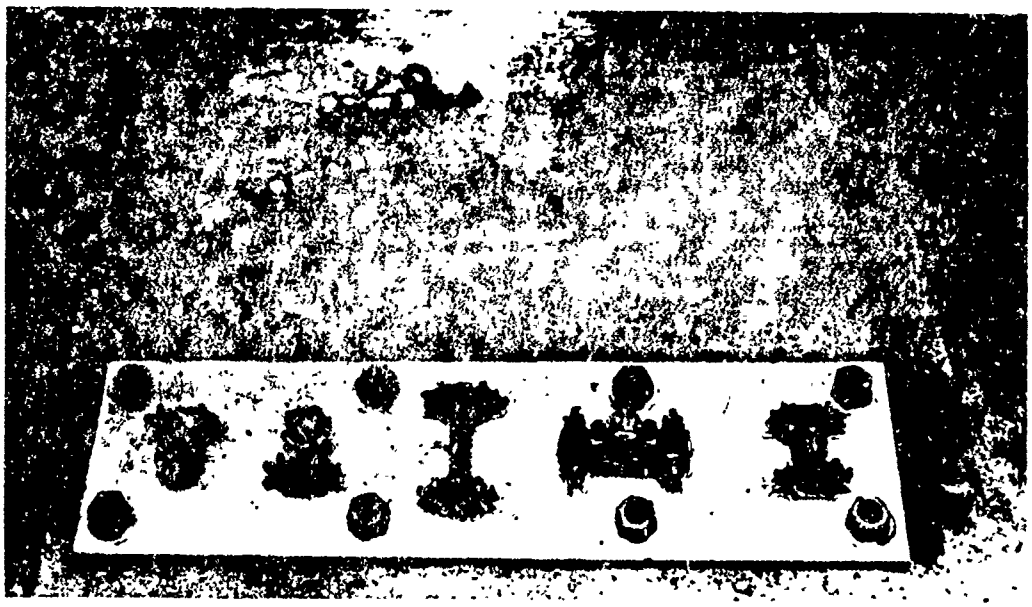

Figure 2.5 Sample station for Shot Cherokee. From left to right on the steel plate can be seen a 1-cm fission ball, 2-cm fission ball, gold holder, special sulfur holder, and zirconium holder. Clamped to the cable are seen the chemical dosimeters.

After irradiation, the activity of the foils was measured on scintillation counters. This counting system in block form is shown in Figure 2.7 and is discussed in the section on fission detectors. In using this system for gold, the samples were held by $\frac{1}{16}$-inch aluminum plate, which was sufficient to shield the beta emissions. The system was biased at 300 kev, which allowed adequate measurement of the 411 kev gamma with a reasonable background count.

Sufficient data were taken to establish a decay curve for each sample. The counting rate at time of irradiation was determined by the following equation:

$$N_{t_0} = N_t \exp\left[-\lambda_g (t - t_0)\right] \tag{2.1}$$

Where: λ_g = Au^{198} decay constant

N_{t_0} = initial counting rate at time t_0

N_t = counting rate at time t

Standard counting techniques were used and the thermal-neutron flux was calculated as follows:

$$\text{Flux} = K(N_{t_0} \text{ bare} - 1.025\, N_{t_0} \text{ shielded}) \tag{2.2}$$

Where: N_{t_0} = the initial counting rate

K = the calibration number

The factor 1.025 is a correction for the epithermal neutrons absorbed by the 0.045-inch thick cadmium shield (Reference 18).

2.5.2 Gold Neutron Detector Calibration. Originally, two separate calibrations of the gold detector system were made. The first calibration was accomplished prior to the field phase of the operation using the thermal column of the X-10 graphite reactor at ORNL as a neutron source. The second calibration was made during the field operation using the Omega water boiler reactor at the Los Alamos Scientific Laboratory (LASL).

For the first calibration, the gold samples in their containers were irradiated for approximately five minutes in the thermal column of the X-10 graphite reactor. The thermal neutron flux was measured by personnel from the Health Physics Division of ORNL with their previously calibrated gold system. The procedure for determining the initial counting rate of calibration samples was the same as that described in Section 2.5.1. The length of time of irradiation was short compared with the half life of Au^{198}; therefore, no correction for decay during irradiation was required. The measured thermal flux was 9.28×10^9 n/cm^2 and the initial counting rate was 1.79×10^4 counts/min. The resulting calibration number was 5.18×10^5 n/cm^2/(counts/min). The accuracy of the neutron flux determination was quoted as ± 6 percent. The counting accuracy was ± 1 percent. An error of indeterminable magnitude existed in positioning the project gold sample, relative to that of the ORNL sample in the thermal column. It was estimated, however, that the error was probably not greater than 10 percent.

The second calibration was accomplished by irradiation of the gold samples in their container in the south thermal column of the Omega reactor at LASL. The samples were located adjacent to the curtain position with the curtain up. The quoted thermal neutron flux was 6.44×10^{11} n/cm^2. The samples were flown to the Eniwetok Proving Grounds (EPG) where the initial counting rate was established as above. The initial counting rate was 1.10×10^6 counts/min. The resulting calibration number was 5.85×10^5 (n/cm^2)/(counts/min). The uncertainty quoted in the neutron flux was approximately 20 percent.

In addition, a third calibration was performed at LASL in April 1957, and the resulting cal-

ibration numbers of the two runs were 6.00×10^5 and 5.83×10^5(n/cm^2)/(counts/min). Subsequent calibrations at LASL in the spring and fall of 1958 (Reference 32) also yielded similar results. Therefore, an average calibration number of 6.07×10^5(n/cm^2)/(counts/min) has been calibrated from the eleven individual calibrations taken and is used in this report.

2.5.3 Fission Threshold Detector. G.S. Hurst and others (Reference 14) of ORNL have developed a method of using Pu^{239}, Np^{237}, and U^{238} as neutron threshold detectors. The isotope Pu^{239} does not have a naturally occurring energy threshold for fission above thermal energies; however, a threshold can be produced by shielding the Pu^{239} with elemental B^{10}. The isotopes Np^{237} and U^{238} have energetic thresholds for the fission process. The gamma rays given off by the fission products can be used as a measure of the number of fissions produced in the exposed materials.

Plutonium, neptunium, and uranium in the form of foils were placed in steel spheres. These spheres were constructed in such a way that it was possible for the periphery to be filled with B^{10}. Extreme care was taken to shield against thermal neutrons. The shield was designed so that an incoming neutron had to penetrate the required thickness of boron, regardless of its direction. Further, the cavity inside the shield was lined with 0.025 inch of cadmium, so that neutrons moderated in the shield were captured before entering the foils. The fission samples were sealed in very thin (0.005-inch) copper dishes to facilitate handling. One-centimeter and two-centimeter B^{10} shields were used, thus giving two separate thresholds for the Pu^{239}. The average density of the 1-cm shields was 1.165 gm/cm^3 and for the 2-cm shields was 1.140 gm/cm^3.

The calculated effective cross section of Pu^{239} shielded with 1 cm and 2 cm of B^{10} with the above densities is shown in Figure 2.6 along with the Np^{237} and U^{238} cross sections (Reference 17). The effective cross section for Pu^{239} is defined as:

$$\sigma_{EFF} = \sigma_F \exp(-\sigma_B N_B) \tag{2.3}$$

Where: σ_F = the fission cross section of Pu^{239}

σ_B = the cross section of the B^{10} (n, α) Li^7 reaction

N_B = the number of B^{10} atoms/cm^2 in the shield

The cross section σ_B is given in Reference 19. The effective threshold (by definition the energy where the cross section is one half of its maximum value) for the 1-cm shield was 500 ev and for the 2-cm shield was 10 kev.

The foils were counted using scintillation techniques, and the natural radioactivity of the samples was determined prior to irradiation. The scintillation apparatus consisted of 1 by 1½-inch NaI (Tl) crystals, Type 5819 photomultiplier tubes, standard preamplifiers and linear amplifiers, and scalers. Figure 2.7 is a block diagram of the system. The crystals were covered with a ⅛-inch brass plate machined to hold the foils. The system was biased at approximately 1.1 Mev using the Co^{60} source as a standard. This method was accurate and convenient.

The fission decay curve for each sample was determined and extrapolated to a time 10 hours after irradiation.

The neutron flux was then determined by:

$$\text{Flux} = K_f CR_t \tag{2.4}$$

Where: K_f = the calibration number determined from the calibration decay curve at 10 hours after irradiation for Pu^{239}, Np^{237}, or U^{238}.

CR_t = the counting rate of Pu^{239}, Np^{237}, or U^{238} samples at 10 hours after irradiation

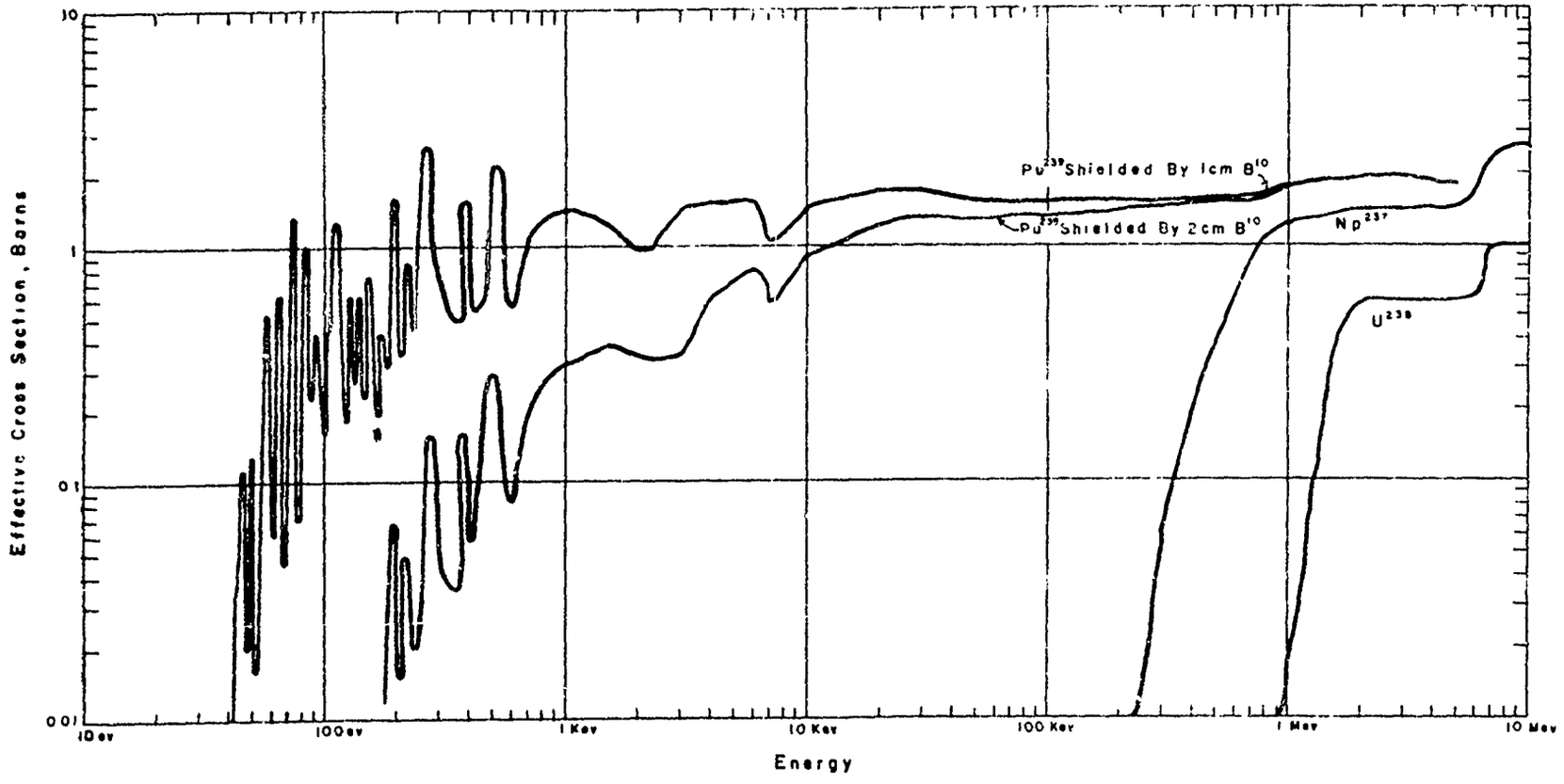

Figure 2.6 Effective Pu^{239}, Np^{237}, and U^{238} fission cross sections.

2.5.4 Fission Detector Calibration. The original calibration of the fission-detector system was accomplished at ORNL. The plutonium samples were irradiated in the thermal column of the X-10 graphite reactor. Three unshielded Pu^{239} samples were exposed in the thermal column for approximately five minutes. The thermal neutron flux in the column at the time of irradiation was measured by using the standard gold detector method. Two of the samples irradiated were 1.58

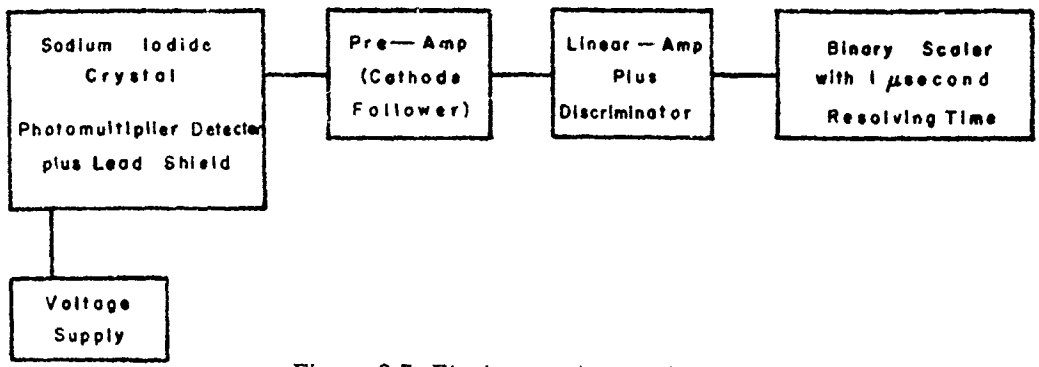

Figure 2.7 Fission counting system.

grams while the other was 0.1 gram. The 0.1-gram sample was used to minimize the effect of absorption of the thermal flux by the plutonium sample. The 1.58-gram samples were used to obtain the decay curve at long times after irradiation. The Pu^{239} samples were counted and the decay curve plotted. The 1.58-gram-sample data were normalized to those of the 0.1-gram

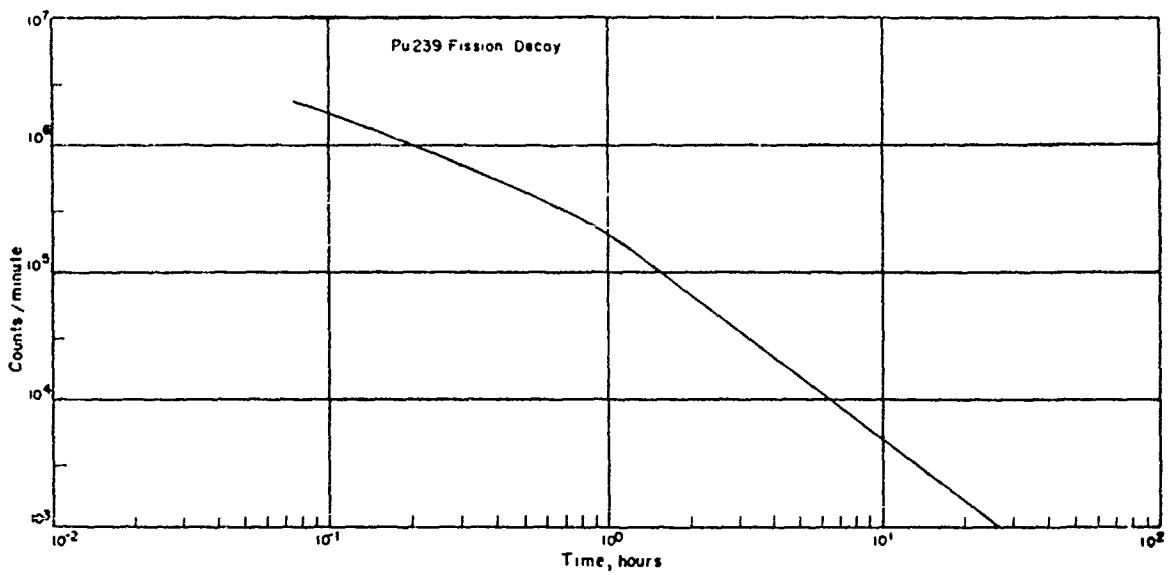

Figure 2.8 Gamma decay curve for 0.1-gram Pu^{239} sample.

sample. Figure 2.8 is the decay curve obtained, and corresponds to the irradiation of 0.1 gram of bare Pu^{239} to 3.11×10^9 thermal-energy neutrons/cm^2.

By using the ratio of the thermal fission cross section for Pu^{239} and the maximum fission cross sections (Reference 14) of B^{10} shielded Pu^{239}, Np^{237}, and U^{238}, it was determined that the curve shown in Figure 2.8 would be obtained from the irradiation of 0.1-gram samples of B^{10} shielded

Pu^{239} by 1.36×10^{12} neutrons/cm^2, of Np^{237} by 1.78×10^{12} neutrons/cm^2 and of U^{238} by 4.53×10^{12} neutrons/cm^2.

For convenience, the calibration number was determined only at 10 hours after irradiation and for a 1.58-gram sample. The calibration numbers were:

Sample	K_f
Pu^{239}	1.61×10^8 (neutrons/cm^2)/cpm
Np^{237}	2.11×10^8 (neutrons/cm^2)/cpm
U^{238}	5.36×10^8 (neutrons/cm^2)/cpm

Five additional calibrations of the fission detectors have been made since the completion of Operation Redwing. The resulting calibration numbers, along with those listed above have been averaged and were used in this report. The calibration numbers were determined for the same conditions as mentioned above (i.e., for 10 hours after irradiation and for a 1.58-gram sample) and were as follows:

Sample	K_f
Pu^{239}	1.58×10^8 (neutrons/cm^2)/cpm
Np^{237}	2.06×10^8 (neutrons/cm^2)/cpm
U^{238}	4.89×10^8 (neutrons/cm^2)/cpm

2.5.5 Sulfur Threshold Detector. The reaction of interest is S^{32} (n, p) P^{32}. The P^{32} decays with the emission of 1.7 Mev beta particles with a 14.3-day half life. This reaction has an effective threshold (i.e., the energy where the cross section for this reaction is one-half its maximum value) at approximately 3 Mev. The cross section for this reaction is shown in Figure 2.9 (Reference 17).

Sulfur samples in the form of pellets were used. Two grams of sublimed sulfur were pressed under a pressure of 10,000 psi to form a 1-inch diameter, $\frac{1}{8}$-inch-thick pellet. The pellets formed in this manner were then placed with approximately 80 grams of loose flowers of sulfur in polyethylene bags. The bags were sealed and, in turn, placed inside the $1\frac{1}{2}$-inch-diameter, 6-inch long pipe nipples used as field holders. A mounting web was welded to the outside of the pipe nipple, which allowed the holder to be attached to the cable or pipe stations by U bolts.

After irradiation, the sulfur pellets were counted by using standard GM tubes and associated equipment. Figure 2.10 is a block diagram of the equipment used.

If the activity of the pellet was too low to measure, the loose sulfur (that which was packed around the pellets) was used to obtain a measurement. Forty grams of the loose sulfur were melted and poured into a cylindrical mold. The cylinders were counted in an anti-coincidence unit which had a low background (approximately 4 counts/min). Figure 2.11 is a block diagram of this unit.

Standard counting procedures were used and corrections were made for coincidence loss within the equipment. Sufficient data were taken to establish a decay curve for each sample. This was done in order to assure that the correct activity was being measured. The counting rate was extrapolated to the time of irradiation by:

$$N_{t_0} = N_t \exp\left[+\lambda_p (t - t_0)\right] \qquad (2.5)$$

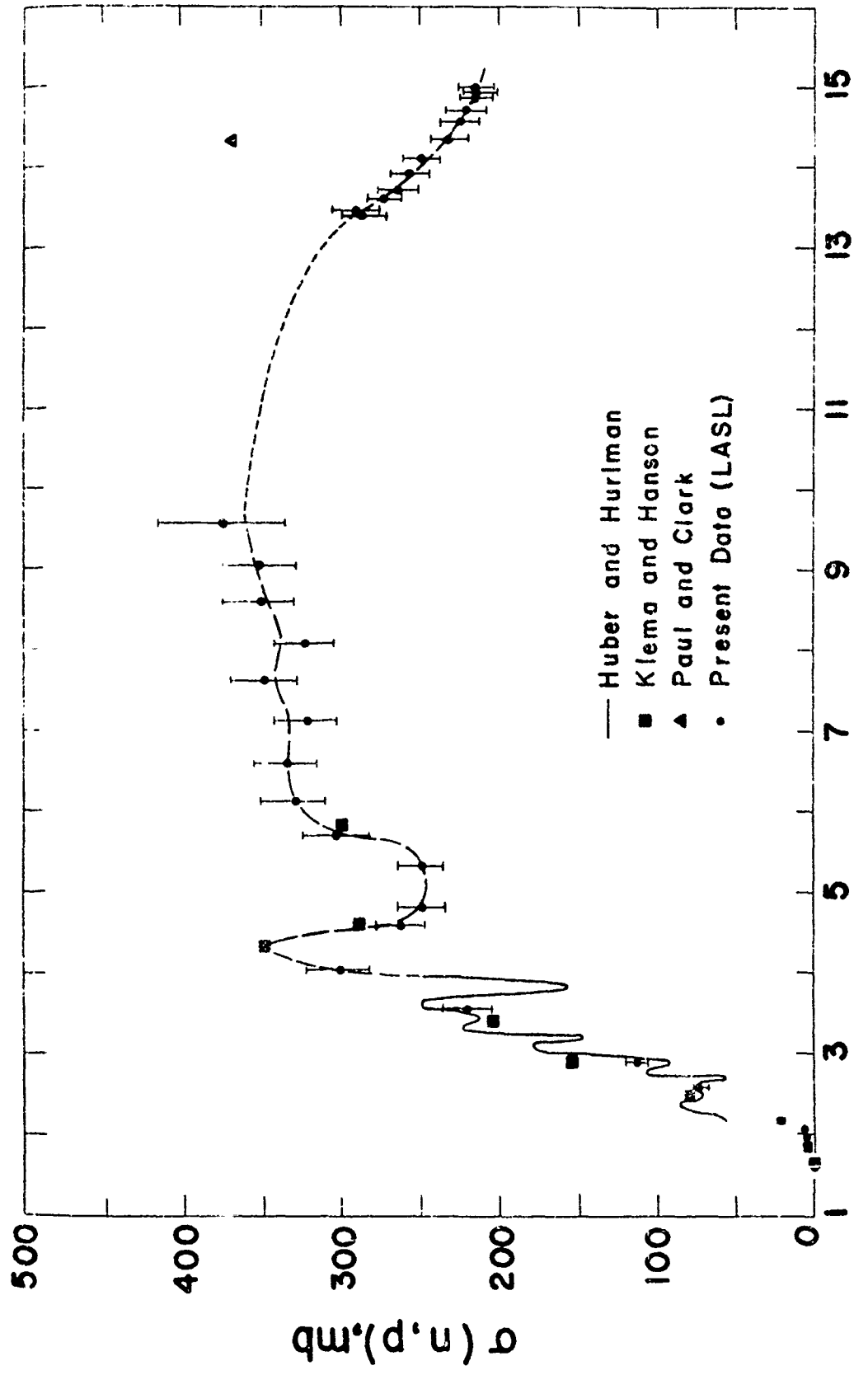

Figure 2.9 S^{32} (n, p) P^{32} cross section (Reference 17).

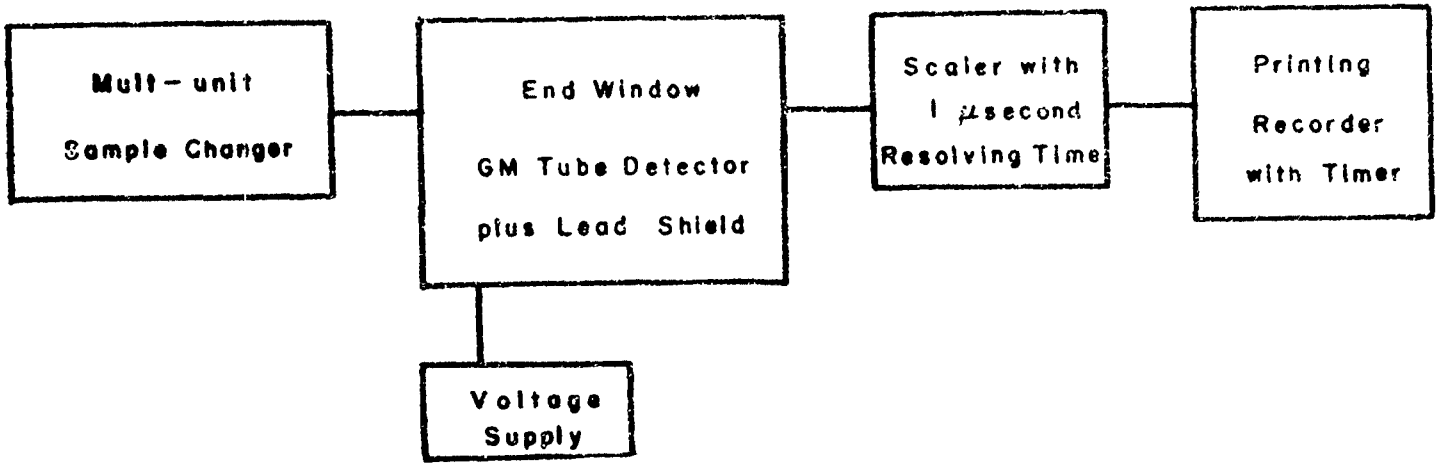

Figure 2.10 Sulfur pellet counting system.

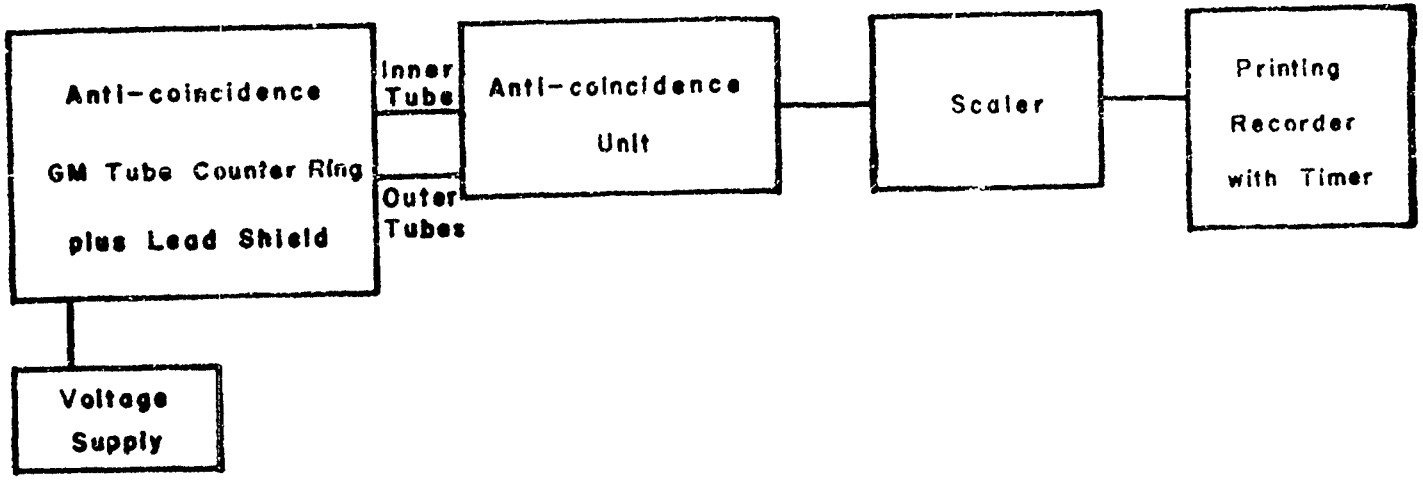

Figure 2.11 Sulfur anticoincidence counting system.

Where: λ_p = P^{32} decay constant

N_{t_0} = counting rate at time t_0

N_t = counting rate at time t

The neutron flux was calculated as follows:

$$\text{Flux} = K_S N_{t_0} \tag{2.6}$$

Where: K_S = the sulfur calibration number

2.5.6 Sulfur Detector Calibration. The only sources of neutrons which had been used for calibration of the sulfur neutron-detector system were the 14.2-Mev neutrons produced by the (d, t) reaction in the Cockroft-Walton accelerator at LASL (Reference 32). The sources consisted of zirconium foils impregnated with tritium. The Cockroft-Walton ion source was radio-frequency-ionized deuterium. The energy of the accelerated deutrons was approximately 250 kev.

The reaction used to form the neutrons was:

$$_1D^2 + {}_1T^3 \longrightarrow {}_2He^4 + {}_0n^1$$

The number of neutrons produced was measured by monitoring the number of alpha particles at a detector with a known geometry.

Two calibration runs were made during the operation at the EPG. The sulfur samples in their field containers were placed approximately in the 60-degree plane of the Cockroft-Walton neutron source. The samples were irradiated for eight, 10-minute intervals spread over a time of approximately five to six hours. This procedure gave a reasonable counting rate in the sulfur. The sulfur samples were then flown to the EPG where they were counted. The counting procedures used were the same as indicated above. No correction for the time of irradiation was required, since this time was short compared to the half life of the P^{32} formed.

The accuracy of the alpha-particle counting was quoted as ± 1 percent; the accuracy of the counting of the sulfur samples ± 2 percent. The accuracy of the measurement of the distance of the sulfur samples from the target was not determined.

2.5.9 Chemical and Germanium Dosimeters. The Air Force and the AEC-UCLA chemical dosimeters included three main types of chemical systems. All were based on the same principle; the amount of acid formed from irradiation of a chlorinated hydrocarbon is a linear function of radiation dose throughout a broad range (25 to 100,000 r), References 19, 20, 21, and 22.

All of the dosimeters were read directly by observing the color changes in the indicator dye. The color change in most instances was from red (pH 6.0 or above) to yellow (pH 5.6 or below), and since the color transition of the overlying dye is a function of dose, exposure doses were estimated by color comparison with irradiated controls.

The over-exposed dosimeters (pH 5.6 or below) were evaluated by measuring the amount of

acid formed per milliliter of chlorinated hydrocarbon. This was accomplished by titrating the acid solution against standardized 10^{-3} normal NaOH. The dose in r was then obtained by comparing the amount of acid formed in the sample under consideration, to that formed by the irradiation of similar samples by known quantities of gamma radiation emitted by a Co^{60} source.

Differential-hydrogen-content chemical dosimeters were used to estimate the fast-neutron dose in rep. This technique was based on the ability of a relatively high-hydrogen-content dosimeter to respond to both gamma rays and fast neutrons and for a hydrogen-free dosimeter to respond to only the coexistent gamma rays (Reference 19). These systems were calibrated by G.S. Hurst and P.S. Harris (Reference 5).

The measurement of neutron dose with the hydrogen-content dosimeter was accomplished by evaluating the number of milliequivalents of stable acid produced in a mixed radiation field. Since the water-equivalent-high-hydrogen-content dosimeter is X- and gamma-ray energy dependent and has a known neutron response, the total acid production can be considered as a function of the combined neutron and gamma radiations. Subtracting the gamma generated acid as measured by the fast-neutron-insensitive chemical dosimeter system (Reference 20) yielded the quantity of acid produced by the neutrons. By dividing the neutron-generated acid by the acid yield/rep of neutron radiation, the neutron dose was obtained.

For Operation Redwing, gamma measurements in the presence of neutrons were accomplished using both anhydrous-chloroform and tetrachloroethylene fast neutron-insensitive systems. Data reported by the Air Force was collected using primarily the anhydrous-chloroform system. Corrections for the thermal-neutron sensitivity of this system [namely, 6.7×10^{-10} rep/(neutrons/cm^2)] was small (in most cases <5 percent) and within the limit of experimental error of the thermal-neutron measurements and was, therefore, not applied to the data in this report. No data was obtained with the tetrachloroethylene system since the neutron-sensitive dosimeters were saturated during exposure and, consequently, could not be read. However, it is noteworthy that during the previously mentioned calibration, agreement between the two chemical dosimeter systems was determined at ± 5 percent.

The evaluation of the AEC germanium dosimeters was made by Dr. Cassen of the UCLA Atomic Energy Project.

The U.S. Air Force and Atomic Energy Commission chemical and germanium dosimeters were placed in $1\frac{1}{2}$-inch-diameter pipe nipples of the same construction as those used as sulfur holders. These holders were then clamped to the cable or reef stations. Upon recovery, the samples were mailed to the United States for evaluation.

Chapter 3
RESULTS

3.1 NEUTRON FLUX MEASUREMENTS

3.1.1 Shot Cherokee. No results were obtained from Shot Cherokee, due to the large error in the actual detonation point with respect to the proposed detonation point.

3.1.2 Shot Yuma. The results of the neutron flux measurements from Shot Yuma are summarized in Table 3.1. As indicated in the table, the data obtained for plutonium and uranium when placed in the 1-cm ball have been adjusted to equivalent 2-cm ball data. In the case of plutonium, adjustment was required in order to give sufficient data points for analysis. It was also determined that there was an attenuation of the neutrons with energies above the uranium threshold by the added material in the 2-cm ball. The correction factors of 0.73 for plutonium and 0.92 for uranium were determined experimentally on Shot Kickapoo (Section 3.1.3). Figures 3.1, 3.2, 3.3, and 3.4 show the results of the measurements of the variation of the neutron flux about the device for plutonium, uranium, sulfur, and gold, respectively. The angles indicated on the graphs are the angles made by the instrument lines with respect to the projection of the long axis of the device on the ground.

The neptunium data were not plotted, as only two data points were obtained on this shot. The validity of the neptunium value at Station 253.15 is in doubt. It is much too low when compared with the neptunium data at Station 253.02. This can probably be attributed to the small amount of induced radioactivity observed in the neptunium sample at this station, thus producing very poor counting statistics.

The straight lines drawn through the plotted points are based on a least-squares analysis of the data and a common slope between detectors on a given line. This will be discussed in Chapter 4. The dotted lines connect those points not used in the least-squares analysis. No extrapolation of data toward the zero point has been attempted, in accordance with suggestions made in the Appendix.

The thermal-neutron data in Figure 3.4 have been plotted in the same manner as the fast-neutron data for reasons discussed in Section 1.3.2. The variation of the thermal flux with angle about the device was small, hence only one line was drawn through the data points.

3.1.3 Shot Kickapoo. The results of the neutron-flux measurements for Shot Kickapoo are given in Table 3.2. Both 1-cm and 2-cm fission balls were placed at Stations 253.25 and 253.45. The conversion factors used to adjust the 1-cm ball data to that of the 2-cm ball data were determined from these data. The average conversion factor for plutonium was 0.73, and for uranium 0.92. Verification of these factors and an indication of the validity of their use is shown by the consistency of the converted 1-cm ball data when plotted with 2-cm ball data. Remarks made in Section 3.1.2 also apply to these data. Figures 3.5, 3.6, 3.7, and 3.8 show the results of the measurements of the neutron flux variation about the device. Again, all statements made in Section 3.1.2 about the graphs apply. The neptunium data were not plotted, since only three consistent points were obtained. The neptunium value at Station 253.27 is very low when compared with the three other points.

3.1.4 Shot Erie. The results of the neutron flux measurements for Shot Erie are given in

Table 3.3. Only two stations could be instrumented with fission detectors. These results are shown in Figures 3.9, 3.10, and 3.11. The extrapolation of these data is based on the result that, for a given instrument line, the semilog plots of the data from all detectors will have a common slope. This will be discussed in Chapter 4. A best-fit curve has been drawn through all thermal neutron data in Figure 3.11.

3.1.5 Shot Blackfoot. The results of the neutron flux measurements for Shot Blackfoot are given in Table 3.4. The data at Station 255.01 are those obtained from the detectors placed in the concrete boxes listed in Section 2.4. Insufficient plutonium and uranium detectors prevented complete instrumentation of these boxes.

Figures 3.12 and 3.13 show the results from Shot Blackfoot. No explanation can be given for the results of measurements made at Stations 252.09 and 252.11. The remaining data have been checked against the results of Program 12 measurements and show excellent agreement.

Again in Figure 3.13 a best-fit curve has been drawn through the thermal-neutron data.

3.1.6 Shot Osage. The results of the neutron flux measurements for Shot Osage are given in Table 3.5 and shown in Figures 3.14 and 3.15. No reasonable explanation can be given for the uranium and neptunium results at Station 5S.

3.2 NEUTRON AND GAMMA-RAY-DOSE MEASUREMENTS

3.2.1 Shot Cherokee. No results were obtained for Shot Cherokee.

Pgs. 37 & 38 Deleted.

3.2.2 Shot Yuma. The results of the neutron dose measurement from Shot Yuma are given in Table 3.6.

The shortage of neptunium required a change in the procedure from that indicated in Section 1.3.3 for calculating the threshold-detector neutron dose. Where neptunium data was available, the dose was determined using the following equation:

$$D = [1.0\,(N_{Pu\ 2cm} - N_{Np}) + 2.5\,(N_{Np} - N_U) + 3.2\,(N_U - N_S) + 3.9\,N_S] \times 10^{-9} \quad (3.1)$$

Where: $N_{Pu\ 2cm}$ = the number of neutrons/cm^2 either measured directly by the plutonium in the 2-cm boron shields or that extrapolated from the measurement made in 1-cm boron shields.

The remaining terms are the same as indicated in Equation 1.3.

The thermal-neutron dose has been neglected, since it can be shown to be insignificant when compared to the total dose. Wherever neptunium data was not available, the following equation was used.

$$D = [1.8\,(N_{Pu\ 2cm} - N_U) + 3.2\,(N_U - N_S) + 3.9\,(N_S)] \times 10^{-9} \quad (3.2)$$

 Pgs 40 thru 42 Deleted.

where the factor 1.8 was determined at the average energy between the effective thresholds of the 2-cm boron-shielded plutonium detector and the uranium detector. In those cases where the uranium data is missing, (i.e., Stations 253.11, 253.13, and 253.20) figures were obtained from the lines drawn to represent the data plotted in Figure 3.2.

The results reported in Table 3.6 for the threshold-detector dose were calculated using Equation 3.2. The AEC germanium calibration curve was double-valued between 0 and 27,000 rep resulting in the possible assignment of two dose values in this region. The second values are reported in parentheses in Tables 3.6, 3.7, and 3.12. No neutron results were obtained from the AEC chemical dosimeters due to saturation of the neutron-sensitive dosimeter.

The gamma-ray dose measurements which are determined in conjunction with the measurement of the neutron dose by chemical methods are reported in Table 3.7 for Shot Yuma. Again, difficulty was experienced with the AEC chemical dosimeters, resulting in only approximate values, as indicated.

Pgs 44 thru 47 Deleted.

Figure 3.16 is a comparison of the neutron dose measurements for Shot Yuma. The threshold-detector results are calculated from the flux data; therefore, no data points have been shown. The angles indicated refer again to the angle the instrument lines make with respect to the projection of the long axis of the device on the ground.

3.2.3 Shot Kickapoo. The results of the neutron dose measurements for Shot Kickapoo are given in Table 3.8. The same remarks made in Section 3.2.2, pertaining to the threshold detector, apply. Only one instrument line included AEC germanium dosimeters; again double values are given. Table 3.9 summarizes the gamma ray measurement for this shot. Figure 3.17 shows the comparison of the different detector results. As above, the angles refer to the projected axis of the device on the ground.

3.2.4 Shot Erie. Table 3.10 gives the results of neutron dose measurements for Shot Erie. No AEC chemical or germanium dosimeters were used on this shot. The gamma results are listed in Table 3.11.

Figure 3.18 compares the threshold-detector neutron dose measurement with the chemical dosimeter neutron measurement.

3.2.5 Shot Blackfoot. The neutron dose results are given in Table 3.12. Since no neptunium samples were available for this shot, the method used in Section 3.2.2 was used to calculate the threshold detector dose. All other remarks pertaining to the AEC germanium and chemical dosimeters also apply to these results. Again the boxes listed at Station 255.01 refer to the concrete boxes as listed in Section 2.4.

The gamma-ray dose measurements are listed in Table 3.13.

TABLE 3.8 RESULTS OF NEUTRON DOSE MEASUREMENTS FOR SHOT KICKAPOO

Station Number	Slant Distance	Threshold Detector	USAF Chemical Dosimeter	AEC Germanium Dosimeter
	yd	rep	rep	rep
253 22	144	—	—	—
253 23	224	5.56×10^5	4.8×10^6	—
253.24	316	2.03×10^5 *	1.4×10^5	—
253.25	413	7.61×10^4	4.8×10^4	—
		8.20×10^4 †		
		7.81×10^4		
		8.32×10^4 †		
253 26	511	3.10×10^4 *	1.4×10^4	—
253.27	610	1.31×10^4	6.4×10^3	—
		1.19×10^4 †		
253 28	709	6.09×10^3 *	3.2×10^3	—
253 29	807	2.52×10^3	1.5×10^3	—
253.32	144	—	—	—
253 33	224	5.06×10^5	4.5×10^5	—
253 34	316	1.78×10^5 *	1.2×10^5	—
253.35	413	6.70×10^4	3.7×10^4	—
253 36	511	2.67×10^4 *	(Lost)	—
253 37	610	1.19×10^4	4.8×10^3	—
253.38	709	5.18×10^3 *	2.1×10^3	—
253 39	807	2.54×10^3 *	—	—
253.40	905	—	—	—
253 42	144	—	—	—
253 43	224	4.05×10^5	3.7×10^5	—
253.44	316	1.29×10^5 *	9.6×10^4	—
253.45	413	4.79×10^4	2.3×10^4	3.7×10^4
		5.06×10^4 †		
		4.67×10^4		
		5.00×10^4 †		
253 47	610	8.27×10^3 *	4.0×10^3	1,500 (2.2×10^4)
253.48	709	3.84×10^3	2.0×10^3	900 (2.5×10^4)
253 49	807	1.79×10^3 *	—	500 (2.7×10^4)
253 50	905	8.89×10^2	—	(2.8×10^4)
		9.75×10^2		
253 51	1,005	4.50×10^2 *	—	—

* Dose calculated by extrapolation of available data.

† Dose calculated using Np data.

Pg. 50 Deleted.

TABLE 3.9 RESULTS OF GAMMA RAY MEASUREMENTS FOR SHOT KICKAPOO

Station Number	Slant Distance	USAF Chemical Dosimeter	AEC Chemical Dosimeter
	yd	r	r
253 22	144	—	—
253.23	224	2.7×10^5	4.1×10^5
253.24	316	1.0×10^5	1.35×10^5
253.25	413	4.8×10^4	1.92×10^4
253.26	511	2.4×10^4	9.0×10^3
253 27	610	1.3×10^4	4.0×10^3
253 28	709	6.4×10^3	4.0×10^3
253 29	807	3.8×10^3	4.0×10^3
253 32	144	—	7.2×10^5
253 33	224	2.4×10^5	2.15×10^5
253.34	316	8.5×10^4	3.43×10^4
253 35	413	4.3×10^4	1.08×10^4
253 36	511	2.0×10^4	—
253.37	610	1.0×10^4	4.0×10^3
253 38	709	6.8×10^3	4.0×10^3
253.39	807	4.0×10^3	5×10^2
253.40	905	2.4×10^3	—
253 42	144	—	—
253.43	224	2.32×10^5	3.5×10^5
253.44	316	8.0×10^4	1.0×10^5
253 45	413	3.5×10^4	1.8×10^4
253.47	610	1.0×10^4	4.0×10^3
253.48	709	6.5×10^3	5×10^2
253.49	807	3.8×10^3	—
253.50	905	2.2×10^3	—
253.51	1,005	—	—

TABLE 3.10 RESULTS OF NEUTRON DOSE MEASUREMENTS FOR SHOT ERIE

Station Number	Slant Distance	Threshold Detector	USAF Chemical Dosimeter
	yd	rep	rep
1911.01	328	9.77×10^5	—
1911.02	442	4.88×10^5	—
1210.04	436	3.10×10^5 *	2.58×10^5
1210.05	542	1.17×10^5 *	1.03×10^5
1210.06	655	4.49×10^4 *	4.28×10^4
1210.07	765	1.87×10^4 *	2.24×10^4
1210.08	840	1.05×10^4 *	1.13×10^4
1210.09	983	3.76×10^3 *	1.5×10^3
1210.10	1,091	1.74×10^3 *	2.2×10^3

* Dose calculated by extrapolation of available data

TABLE 3.11 RESULTS OF GAMMA RAY MEASUREMENTS FOR SHOT ERIE

Station Number	Slant Distance	USAF Chemical Dosimeter
	yd	rep
1911.01	328	—
1911.02	442	—
1210.04	436	7.7×10^4
1210.05	542	3.8×10^4
1210.06	655	1.7×10^4
1210.07	765	1.0×10^4
1210.08	840	5.0×10^3
1210.09	983	2.8×10^2
1210.10	1,091	1.7×10^3

TABLE 3.12 RESULTS OF NEUTRON DOSE MEASUREMENTS FOR SHOT BLACKFOOT

Station Number	Slant Distance	Threshold Detector	USAF Chemical Dosimeter	AEC Germanium Dosimeter
	yd	rep	rep	rep
252.01	—	—	—	(Lost)
252.02	—	—	—	(Lost)
252.03	220	—	—	8.0×10^5
252.04	327	8.56×10^5	1.79×10^5	3.9×10^5
252.05	436	3.38×10^5	1.04×10^5	6.8×10^4
252.06	552	1.31×10^5 *	3.4×10^4	3.0×10^4
252.07	656	4.99×10^4	1.4×10^4	9.0×10^3
252.08	769	2.19×10^4 *	5.8×10^3	9.0×10^3
252.09	878	9.97×10^3 *	3.72×10^3	3.0×10^3 (20,000)
252.10	987	5.02×10^3 *	1.48×10^3	2.0×10^3 (22,000)
252.11	1,098	2.56×10^3 *	8.5×10^2	1.5×10^3 (25,000)
255.01	259	—	(Lost)	—
Box 1	259	—	(Lost)	—
Box 2	259	—	(Broken)	—
Box 3	259	—	4.0×10^5	—
Box 4	259	3.65×10^5	3.2×10^5	—
Box 5	259	—	(Lost)	—
Box 6	259	—	2.8×10^5	—

* Dose calculated by extrapolation of available data.

TABLE 3.13 RESULTS OF GAMMA RAY MEASUREMENTS FOR SHOT BLACKFOOT

Station Number	Slant Distance	USAF Chemical Dosimeter	AEC Chemical Dosimeter
	yds	rep	rep
252.01	—	—	—
252.02	—	—	—
252.03	220	—	10^6
252.04	327	8.5×10^4	5.65×10^5
252.05	436	5.4×10^4	3.32×10^6
252.06	552	1.8×10^4	1.10×10^5
252.07	656	8.72×10^3	—
252.08	769	4.51×10^3	10^4
252.09	878	2.6×10^3	4.0×10^3
252.10	987	1.6×10^3	4.0×10^3
252.11	1,098	1.0×10^3	4.0×10^3
255.01	259	(Lost)	—
Box 1	259	(Lost)	—
Box 2	259	7.4×10^5	—
Box 3	259	4.0×10^5	—
Box 4	259	3.8×10^5	—
Box 5	259	(Lost)	—
Box 6	259	5.86×10^5	—

Figure 3.19 gives a comparison of the USAF chemical dosimeter and the AEC germanium dosimeter measurements with the threshold detector dose measurements.

3.2.6 Shot Osage. Table 3.14 summarizes the results of the threshold-detector dose results

TABLE 3.14 RESULTS OF NEUTRON DOSE MEASUREMENTS FOR SHOT OSAGE

Station Number	Slant Distance	Threshold Detector
	yds	rep
1 N	244	4.09×10^5
1 S	237	4.54×10^5
2 S	272	2.86×10^5
3 S	333	1.45×10^5
4 S	411	5.97×10^4
5 S	490	2.07×10^4

for Shot Osage. No chemical or germanium dosimeters were available for this shot. The results of the threshold detector neutron dose calculation are shown in Figure 3.20.

3.3 WEATHER

Weather conditions at the time of detonation of the various devices are given in Table 3.15. No

TABLE 3.15 DETONATION TIME WEATHER DATA

Shot	Sea Level Pressure	Free Air Temperature	Relative Humidity
	mb	°F	pct
Yuma	1,010.2	81.7	80
Kickapoo	1,009.8	85.6	71
Blackfoot	1,012.5	81.1	84
Osage	1,008.5	85.9	74
Erie	1,009.1	80.3	80.2

air-density corrections of the data have been made in this report, since the correction was small (<10 percent), and within the limits of experimental error for the technique used.

3.4 MEASUREMENT OF SCATTERED NEUTRONS

In order to determine the percentage of the measured neutrons which were scattered neutrons, and experiment was devised utilizing a collimator.

The collimator consisted of a piece of steel pipe which was 8 inches in diameter and approxi-

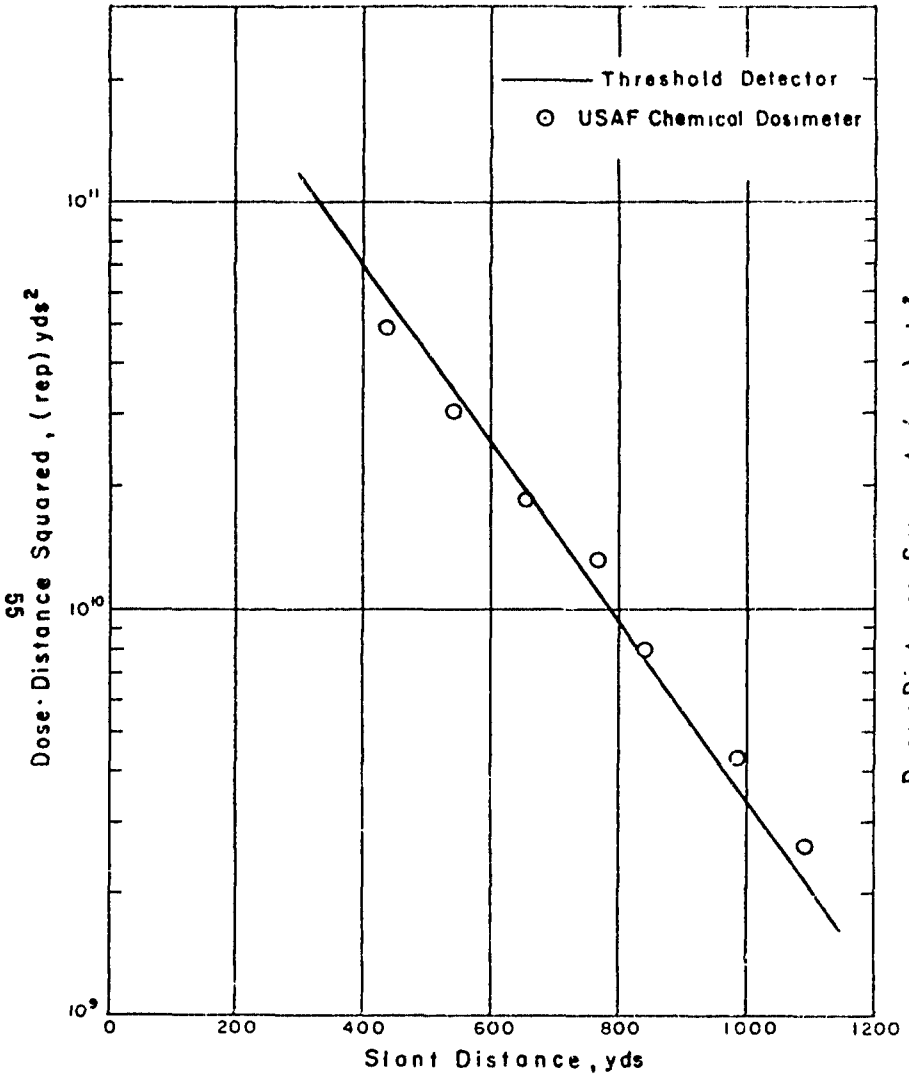

Figure 3.18 Threshold detector and USAF chemical dosimeter neutron dose for Shot Erie.

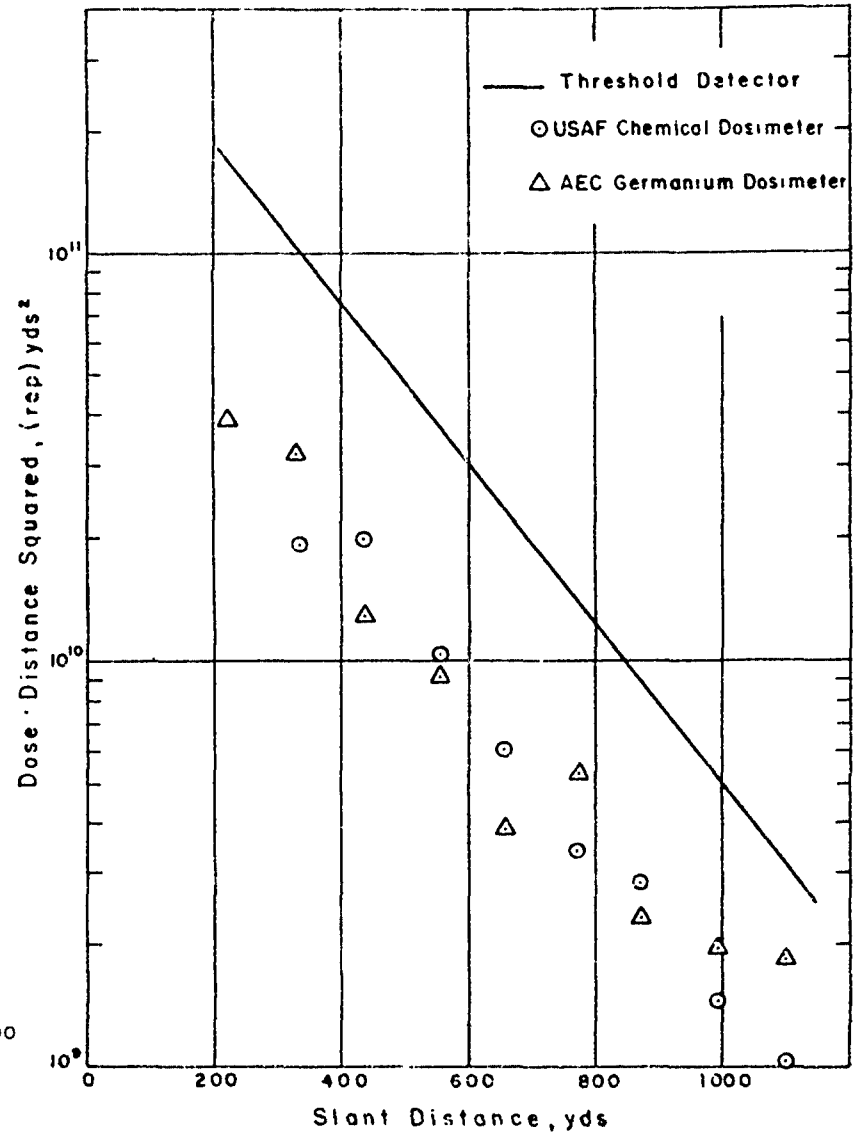

Figure 3.19 Threshold detector, USAF chemical dosimeter and AEC germanium dosimeter neutron dose for Shot Blackfoot.

mately 4 feet long. The pipe was shielded by 3 to 4 feet of sand. A sulfur detector was placed inside the pipe, and another sulfur detector outside the pipe. This array was installed at Shot Kickapoo at a slant distance of 413 yards from the device.

It was concluded that approximately 68 percent of the measured neutrons above 3 Mev at this distance from ground zero were scattered neutrons.

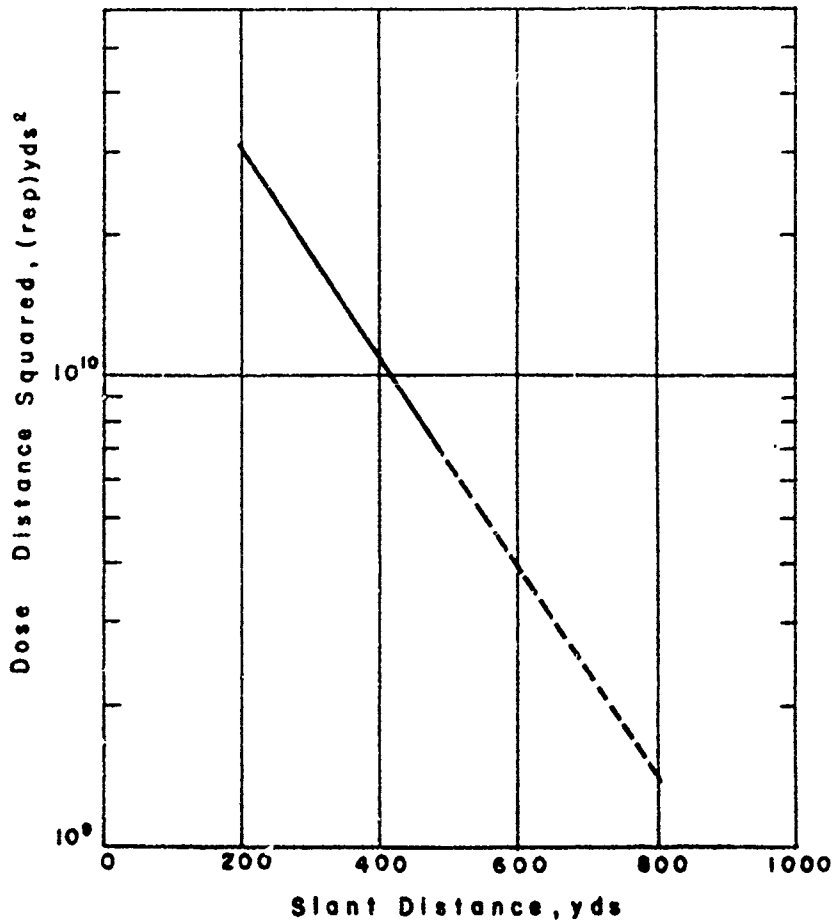

Figure 3.20 Threshold detector dose for Shot Osage.

Chapter 4
DISCUSSION

4.1 NEUTRON SPECTRUM

During the field phase of Operation Redwing, the schedule for Shots Blackfoot and Kickapoo was revised, necessitating a reduction in the planned instrumentation arrays for each event. Due to the limited number of fission detectors available, it was not possible to expose a complete set at each station. Therefore, in most cases, insufficient data were obtained to completely evaluate the neutron spectrum. In addition, the apparent unreliability of some of the neptunium data as indicated in Chapter 3 reduced the probability of reaching positive conclusions regarding the variation of the neutron energy spectrum in the 0.6-Mev region.

Table 4.1 lists the percentage of fast neutrons in the various energy ranges for Shots Kickapoo, Erie, and Osage. These data were obtained by taking an average of the information obtained at the stations which were fully instrumented for these events. The results from Shots Yuma and Blackfoot were also checked and found in good agreement with the values shown in Table 4.1, but are not presented since only plutonium, uranium, and sulfur data were available.

A statistical analysis of the fast neutron data from Shots Yuma, Kickapoo, and Blackfoot showed that the neutron flux-times-distance squared versus distance curves for any one given instrument line had a common slope beyond 300 yards from ground zero. This result indicated that there was no detectable change in the energy spectrum with increasing distance beyond 300 yards from the source. It is possible that the expected variation in spectrum as indicated in the Appendix was not detected, due to a smearing of the data by the non-step-function nature of the detector cross sections, and/or the statistical variation inherent in the measurement system.

As a result of the above analysis, the common slope determined for each instrument line was used in drawing the straight-line portion of the curves in Figures 3.1 through 3.15.

4.2 NEUTRON FLUX MEASUREMENTS

4.2.1 Variation of Neutron Flux about an _____ Device. Table 4.2 summarizes the angular variation of the neutron flux about the two ___ ___ ___ devices. The values listed are the average values of the ratio of the flux times slant distance squared measured on the 64-degree and 85-degree lines to that measured on the 0-degree line for Shots Yuma and Kickapoo, respectively. The data from the straight-line portion of the curves as drawn in the figures in Chapter 3 have been used.

The variation of the 45-degree-line data, both in Shots Yuma and Kickapoo, is quite interesting. In Shot Yuma the apparent decrease in the slope of the 45-degree line, when compared to the slopes of the 0- and 64-degree lines, might be caused by the variation of the quantity of the hydrogenous material on the surface over which the measurements were made. It was noticed during installation of the detectors on the 45-degree line for Shot Yuma that the 100-and 200-yard stations were over a grass-covered surface. Proceeding to the more distant stations, the grass cover decreased until at 500 yards the surface was free of vegetation and consisted mainly of coral sand. If this effect is, in fact, the cause and is as large as indicated by the variation in the slope, it would also explain the large increase in the ratios for uranium and sulfur shown in Table 4.2. The 0-degree line was completely over a grass-covered surface while the 64-degree line was over a sandy surface.

For Shot Kickapoo, it can be seen that the plutonium data for the 45-degree line lies almost on

top of the data for the 85-degree line, while the sulfur and uranium data tend to approach the 0-degree-line data. In this case, the 0-degree line was almost entirely over water; the 45-degree line, except for the first two stations, was over a grass-covered surface; and the 85-degree line was over a sandy surface.

The variation in the thermal-neutron flux with angle about the device also tends to substantiate the above argument. At ranges greater than 300 or 400 yards, the major portion of the thermal-neutron flux is believed to be due to the thermalized fast neutrons which have escaped from the device. The thermal neutrons, thus, are a measure of the total number of fast neutrons present. It is noted that the ratios for the gold detectors are in agreement with the 30-percent variation found for a similar device measured during Operation Teapot.

4.2.2 Data from Stations Close to Ground Zero. Attention is called to the curvature in the lines in Figures 3.1 through 3.4. Shot Yuma afforded the first real opportunity to obtain this close-in data. Part of this curvature is known to be caused by the attenuation of the neutron flux by the tower. A quantitative estimate of this attenuation cannot be made. It is also believed that a portion of the curvature is due to that predicted by the theory as indicated in the Appendix.

4.2.3 Mean Free Path. As mentioned in Section 1.4, the slope of the neutron flux times slant distance squared versus slant distance plot is a measure of the mean free path. For purposes of comparison, these slopes were calculated in the form of e-fold distance (the distance in which the flux is reduced by a factor of 1/e).

Table 4.3 lists the values of the e-fold distances for the various shots of this operation. These values, with the exception of that for the 45-degree line at Shot Yuma, are similar to those made at past operations at the EPG (Reference 12).

4.3 COMPARISON OF THE VARIOUS METHODS FOR DETERMINING NEUTRON DOSE

As can be seen in Figures 3.16 through 3.20, the chemical dosimeters were low by an average

factor of 3.47 for Shot Yuma, 1.76 for Shot Kickapoo, 3.54 for Shot Blackfoot, and ranged from a factor of 1.20 high to a factor of 1.20 low for Shot Erie.

The germaninum dosimeters were low by an average factor of 5.38 for Shot Yuma, 3.68 for Shot Kickapoo, and 3.46 for Shot Blackfoot.

No reason can be given for the inconsistencies in these various systems for measuring neutron dose. However, since the systems have never been directly cross-calibrated, it is possible that future experimentation may either reduce the differences noted, or at least bring about a logical explanation for them.

Similarly, no ready explanation is available for the apparent nonlinearity in the chemical-dosimeter data as ground zero is approached, even though this same phenomena was observed during Operation Teapot.

As in the past, the germanium data are somewhat erratic. The germanium used in this test was known to have a nonlinear response up to 27,000 rep, i.e., a double-valued calibration

TABLE 4.3 THE e-FOLD DISTANCES FROM SHOTS YUMA, KICKAPOO, BLACKFOOT, ERIE AND OSAGE

Shot	e-Fold Distance
	yd
Yuma	
0°	215
45°	218
64°	210
Kickapoo	
0°	203
45°	203
85°	203
Blackfoot	230
Erie	200
Osage	190

curve was observed in this range. This fact indicated that N-type germanium crystals were used.

4.4 NEUTRON AND GAMMA-RAY SHIELDING BY SPECIAL CONCRETES

An analysis of the data given in Table 3.4 indicates that the addition of borax or sulfur does not increase the fast-neutron shielding characteristics of the concrete a sufficient amount to be detected by the threshold detectors. The attenuation of the thermal-neutron flux by the addition of borax to the concrete can be seen by comparing Box 1 with Boxes 3 and 5. Box 1 contained no additives. Box 3 contained 20 pounds of borax added to the water before mixing. Box 5 contained 60 pounds of borax added to the water before mixing. In all cases the boxes consisted of approximately 2,500 pounds of concrete. The ratio of the thermal-neutron flux measured in Box 1 to that measured in Box 3 was 2.8. The same ratio for Box 1 to Box 5 was 7.2. As might be expected, the addition of sulfur to mix had no apparent effect on the thermal-neutron flux.

By extrapolating the threshold-detector-dose data presented in Table 3.12 to 259 yards and comparing this figure to that obtained inside Box 4, which was the only station at which complete data was obtained, it is noted that the neutron dose inside the box was reduced by a factor of approximately four. This factor can be referred to as an estimate of the neutron shielding afforded by a structure of this type.

Similarly, by comparing an extrapolated gamma-dose value to that obtained in Boxes 2, 3, 4, and 6, it is found that the gamma dose inside the boxes was increased by factors of 1.8, 3.3, 3.5, and 2.3 respectively. This resultant increase in gamma dose is in good agreement with the results found at Operation Teapot (Reference 5). The fact that the gamma dose increased due to the presence of the shielding material indicates a possible requirement for the consideration of the induced activities when neutron shields are being designed for equipment such as a tank, or when the shielding characteristics of thin-walled buildings are being considered. Again, no attempt has been made to make more than a semi-quantitative analysis of these data, due to the uncertainties in this particular field measurement; for example, the restricted geometry and the various additives in the concrete.

4.5 COMPARISON WITH PREVIOUS OPERATIONS

Table 4.4 and Figure 4.1 contain information relative to the dose per unit yield versus ground range observed for Operation Redwing Shots Yuma, Blackfoot, Erie, Kickapoo, and Osage;

Operation Teapot Shots Moth, Post, and Wasp, and values predicted in TM 23-200. However, only Shots Yuma, Blackfoot, Kickapoo, and Osage data are beyond the factor of reliability stated in TM 23-200.

It should also be noted that the data from Operation Teapot events has been based on obsolete cross section data. When corrections are made for current data, the dose is increased. An example of this correction may be seen in the Shot Moth data in the table. It is also illustrated by lines H and H′ in the figure.

Table 4.5 shows a comparison of the dose per unit yield data for the aforementioned shots at a slant range of 500 yards and the high-explosive thickness through which the neutrons passed before arriving at the detectors. An inspection of this data will show that there is generally a decrease in the dose per unit yield with increasing high-explosive thickness. Additional measurements and investigations may show a more definite correlation between these parameters.

Pg. 61 Deleted.

Chapter 5
CONCLUSIONS

The conclusions that may be drawn from the measurements made by Project 2.51 are as follows:

No data were obtained during Shot Cherokee because of the difference in the actual and intended ground zero location.

The variation of the neutron flux about the devices fired for Shots Yuma and Kickapoo was energy dependent. The ratios of the neutron flux along a line at 60 degrees to the projection on the ground of the long axis of the device to that along a line at 0 degrees to this projection for Shot Yuma were 1.34, 1.91, 1.94, and 1.18 for the plutonium, uranium, sulfur, and gold detectors, respectively. The same ratios between the 85-degree and 0-degree lines for Shot Kickapoo were 1.62, 1.70, 1.62, and 1.22.

Within the range of the measurements made and the accuracy of the threshold detector system there was no variation of the neutron energy spectrum with increasing distance from the point of detonation.

Any data obtained from an extrapolation of a plot of the neutron flux times slant distance squared versus slant distance to ranges of less than 300 yards may be in error. Theoretical calculations supported by experimental evidence indicate that the relationship is nonlinear in this range.

The neutron-dose results obtained by using the USAF chemical dosimeters were not consistent with those obtained by the threshold detector technique, ranging from a factor of 1.26 high for Shot Erie to an average factor of 3.54 low for Shot Blackfoot.

The AEC germanium dosimeter results were lower by factors of 3.46 to 5.38, than those obtained by the threshold detector technique.

The AEC chemical dosimeter system may not be used to measure neutron dose in the range of 25,000 to 856,000 rep, due to saturation of the neutron-sensitive dosimeter and difficulties inherent in obtaining accurate readings.

There is little or no increase in the attenuation of fast neutrons by adding borax or sulfur to concrete. The attenuation of the thermal-neutron flux is increased by adding borax.

The neutron dose was reduced by a factor of approximately four by a concrete box 3 feet on a side and 6 inches thick, fabricated from a mixture containing 1.6 percent borax by weight. The gamma-ray dose, however, was increased by an average factor of 2.75 by similar concrete boxes containing varying amounts of borax and sulfur.

The measured neutron dose per unit yield was higher for all shots than was predicted by TM 23-200. However, only the Shot Yuma, Blackfoot, Kickapoo, and Osage data falls beyond the factor of reliability stated in the manual.

Appendix A

THEORETICAL SPATIAL DEPENDENCE of the NEUTRON FLUX from a POINT SOURCE

A.1 OBJECTIVE

The objective of this work is to compare the theoretical spatial dependence of the 4π neutron flux from a point source with estimates of this dependence obtained in field tests of nuclear devices. Theoretical calculations are based on numerical solutions of the transport equation for neutrons in air obtained by Holland and Richards (Reference 23).

A.2 THEORETICAL BACKGROUND

The penetration of neutrons in a uniform infinite medium may be calculated by using the moment method for solving the Boltzmann transport equation, this has been done (Reference 23) for monoenergetic isotropic point sources in air. For convenience, the following transport equation for an infinite, plane, isotropic source was solved:

$$\cos\theta \frac{\partial N(x, \cos\theta, u)}{\partial x} = -\mu_T N(x, \cos\theta, u) + \int_{4\pi} d\Omega' \int_0^u du' \; N(x, \cos\theta', u') \mu_e(u') f(u', \cos\theta) \frac{1}{2\pi} \delta$$

$$\left[u-u' - \frac{2}{M}(1 - \cos\phi)\right] + \int_{4\pi}\int_0^u d\Omega' \, N(x, \cos\theta', u') \frac{1}{4\pi} K(u, u') + \frac{\delta(u)\,\delta(x)}{4\pi} \qquad \text{(A.1)}$$

Where:
- N = the neutron flux in a volume element about x per unit solid angle per unit lethargy per unit time, with lethargy between u and u + du and directed within the solid angle $d\Omega$
- θ = the angle between the neutron direction and the normal to the source plane.
- x = the distance from the source plane to the volume element.
- u = the lethargy, $\log(E_0/E)$, where E_0 is the source energy, and E is the neutron energy.
- μ_T = the total neutron cross section for air.
- μ_e = the elastic-scattering cross section.
- $f(u', \cos\theta)$ = the differential angular-scattering cross section for lethargy u'.
- ϕ = the change in angle of neutron direction upon scattering.
- $K(u', u)$ = the differential inelastic-scattering cross section, denoting the probability of scattering from u' to u.

This transformation from point-source geometry to plane-source geometry is possible, since the moments of the function which is the solution of the isotropic point-source problem are simply related to those of the solution to the isotropic plane-source problem (Reference 24).

Following the method of moments, the angular dependence of the neutron flux is removed by expanding N in a series of Legendre polynomials:

$$N(x, \cos\theta, u) = \sum_{i=0}^{\infty} \frac{2i+1}{4\pi} N_i(x, u) P_i(\cos\theta) \qquad \text{(A.2)}$$

After substituting Equation A.2 into Equation A.1, multiplying by an arbitrary $P_j(\cos\theta)$, and integrating over $\cos\theta$ from -1 to +1, the following is obtained:

$$\frac{-1}{2j+1}\left[j \frac{\partial N_{j-1}}{\partial x} + (j+1) \frac{\partial N_{j+1}}{\partial x}\right] + \mu_T N_j = \int_0^u \mu_e(u') N_j(x, u) \frac{M}{2} f\left[u', 1 - \frac{M}{2}(u-u')\right] P_j\left[1 - \frac{M}{2}(u-u')\right]$$

$$du' + \delta_{j0} \int_0^u N(x, u') K(u', u) du' + \delta_{j0}\,\delta(u)\,\delta(x) \qquad \text{(A.3)}$$

The form of the integrand in the first integral term of Equation A.3 follows from the Dirac delta function in the corresponding term of Equation A.1, which requires, in scattering through an angle ϕ, that the energy change of the neutron is fixed such that:

$$\cos\phi = 1 - \frac{M}{2}(u - u')$$

Where: M = the weighted average mass number for nitrogen and oxygen in air.[1]

The presence of the Kronecker delta function, δ_{j0}, in the second term of Equation A.3 follows from the requirement that inelastic scattering be isotropic.

If the moment b_{ln} of the function $N_l(x, u)$ is defined as:

$$b_{ln} \equiv \frac{\bar{\mu}^{n+1}}{n!} \int_{-\infty}^{+\infty} x^n N_l(x, u)\, dx,$$

Where: $\bar{\mu}$ = a standard, reciprocal, mean free path associated with the neutrons of the source energy.

After multiplying by $\bar{\mu}^{n+1} x^n$, integrating over distance, and subtracting the moments for the direct radiation:

$$\mu_T B_{ln}(Z) = \frac{1}{2l+1}\left[l B_{l-1,\, n-1} + (l+1) B_{l+1,\, n+1}\right] + 2\int_0^Z \mu_e(Z') B_{ln}(Z') f\left[Z',\, 1-2(Z-Z')\right] P_l$$

$$\left[1-2(Z-Z')\right] dZ' + \delta_{l0}\frac{4}{M}\int_0^Z B_{0n}(Z')\, K(Z', Z)\, dZ'$$

$$+ \frac{A_l^n}{\left[\mu_T(0)\right]^{n+1}}\left[\frac{M}{2}\mu_l(0) f(0,\, 1-2Z) P_l(1-2Z) + \delta_{l0} K(0, Z)\right] \qquad \text{(A.4)}$$

Where: $A_l^n = \frac{1}{2l+1}\left[l A_{l-1}^{n-1} + (l+1) A_{l+1}^{n-1}\right] + \delta_{n0}\delta_{l0}$

B_{ln} = the moment of the scattered flux only.

In Equation A.4 the lethargy has been linearly transformed to Z, for convenience, such that $Z = \frac{1}{4}\mu$. These equations (A.4) form a linked set of Volterra-type integral equations which may be solved by ordinary numerical methods when experimental and/or theoretical values for the various cross sections are known over the complete energy range of interest.

In general, the moments B_{ln} obtained by solving these equations (A.4) completely determine the scattered neutron flux. In a situation, however, where a single, closed, spatial weight function cannot be used over the full ranges of distance and energy, it becomes difficult to reconstruct this function from its moments by ordinary expansion techniques (Reference 25). The technique used in Reference 23 therefore essentially determined best-fit trial functions and their coefficients from a limited number of computed moments. The trial functions were selected on the basis of correct asymptotic behavior, theoretical one-velocity solutions, and empirical results.

A.3 PROCEDURE AND RESULTS

A.3.1 Neutron Flux. Calculations based on the numerical solution of the transport equation by Holland and Richards (Reference 23) are presented herein for comparison with data from field tests of nuclear devices. These calculations evidently only approximate the actual solutions for neutron transport under field test conditions. The application of these results to field tests ignores the perturbations both in the number of outgoing neutrons from the source and in the shape of their spectrum due to the materials surrounding the fissionable material in an actual bomb. Furthermore, the perturbation of the spatial dependence and magnitude of the neutron flux near the ground is not quantitatively considered.

For the purposes of these calculations, the source spectrum chosen was the Watt fission spectrum.

[1] This treatment assumes scattering from one "average" atom rather than considering the more complicated problem of different elements.

This is admittedly an approximation, its use was quantitatively justified to some extent (as discussed below) by computation of the spatial dependence of neutrons from a source originally of fission shape, but perturbed by traversing a hydrogenous medium. The difficulties involved in comparing calculated results for an infinite air medium to field results from the air-ground interface were resolved by assuming that the effect of the ground on spatial dependence of the flux is unimportant at large distances from the source.

The procedure followed was to evaluate the scattered flux greater than three threshold energies (0.2, 0.7, and 2.5 Mev) for the five source energies which were available from Reference 23 (0.5, 1.0, 2.0, 5.15,

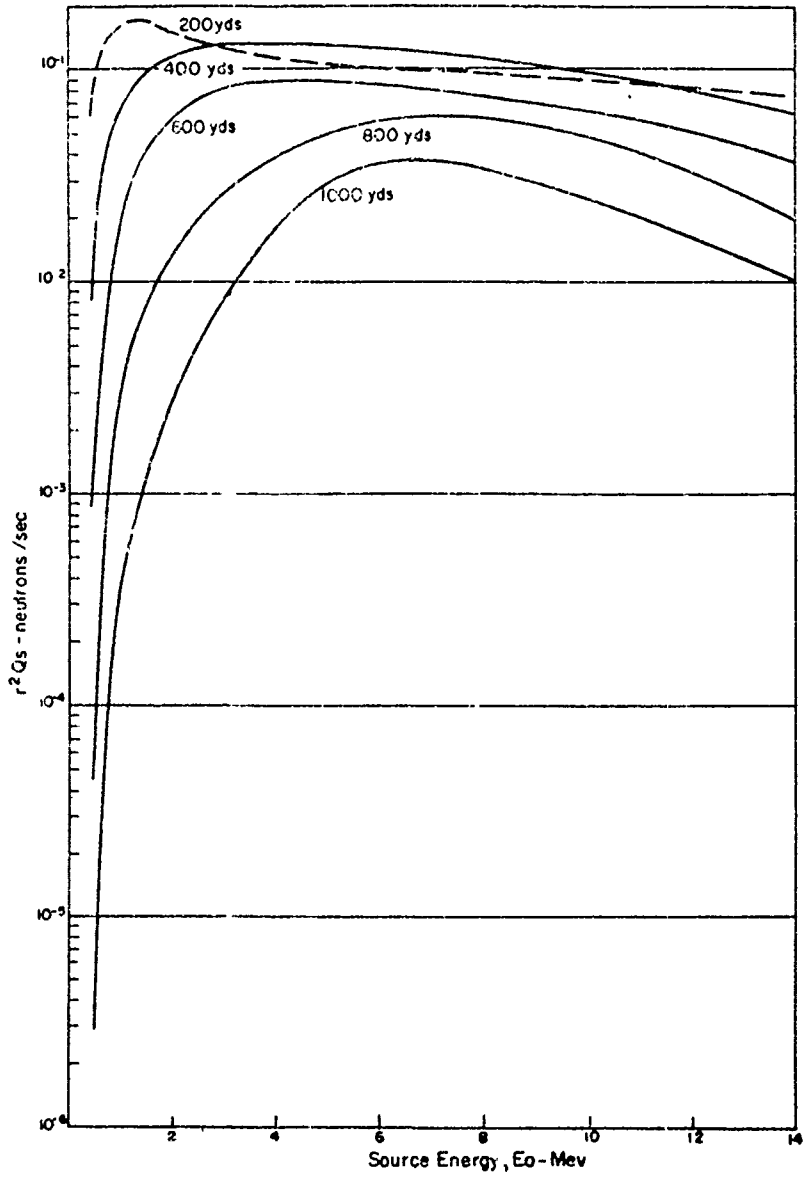

Figure A.1 Plot of scattered portion of the r^2 flux of neutrons with energy greater than 0.2 Mev from a monoenergetic point source, (emitting one neutron/sec) as a function of source energy at various distances from the source.

and 14.0 Mev). The total scattered flux from source energies greater than the above threshold values was obtained as a function of source energy by integrating the spectra for each line source between threshold and source energies. These functions are plotted in Figures A.1, A.2, and A.3 for thresholds of 0.2, 0.7, and 2.5 Mev, respectively. In the case of the 2.5-Mev threshold curves, only two source energies were

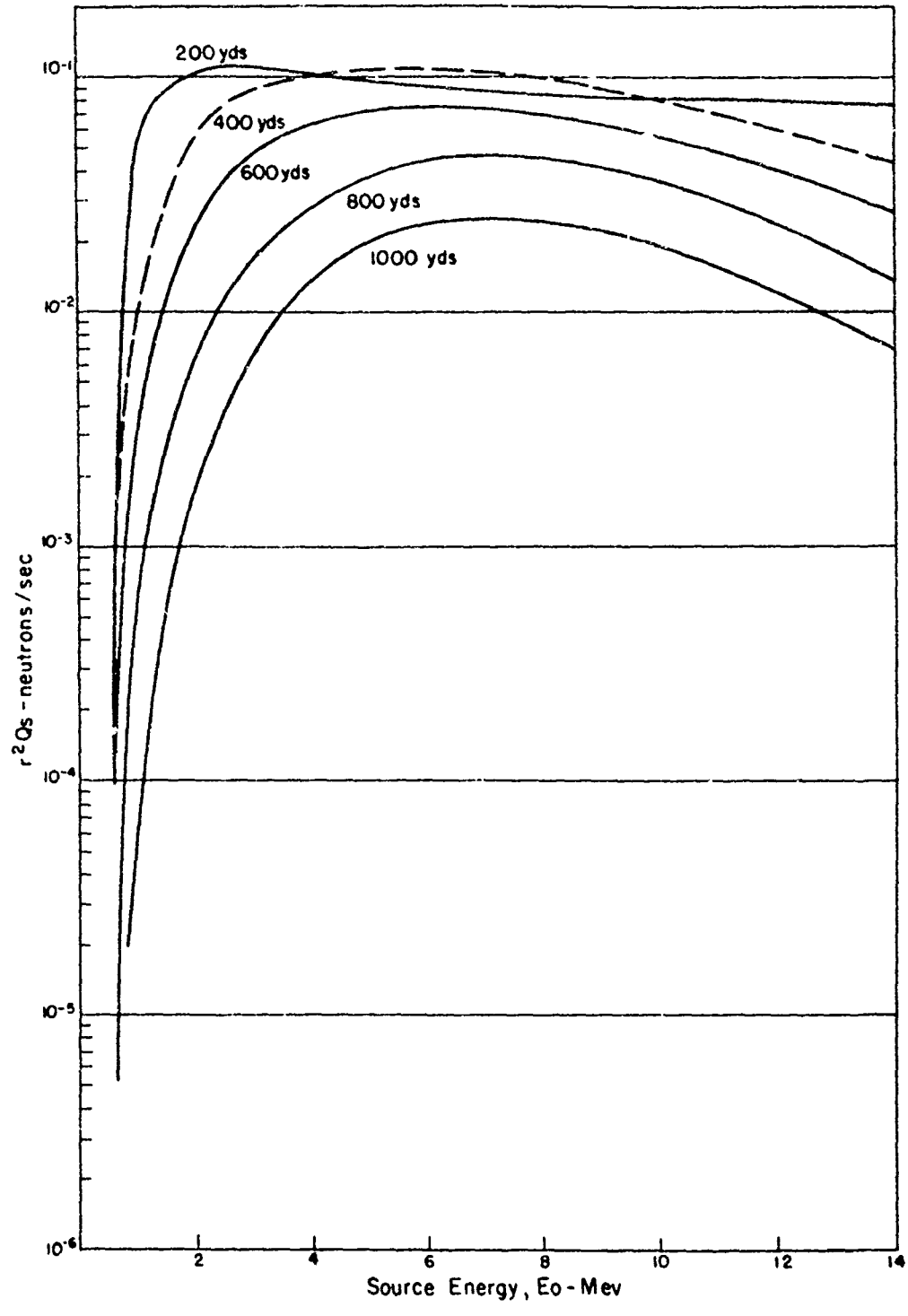

Figure A.2 Plot of scattered portion of the r^2 flux of neutrons with energy greater than 0.7 Mev from a monoenergetic point source, (emitting one neutron/sec) as a function of source energy at various distances from the source.

available, so that the actual curves were approximated by following the same dependence on source energy as exhibited in the two previous cases, guided by the fact that the plotted function must vanish for $E_0 < E_{threshold}$

In order to determine the function r^2 times scattered flux greater than $E_{threshold}$ for neutrons from a point-fission source at various distances from the source, the curves in Figures A.1, A.2, and A.3 were weighted by the normalized fission curve (Reference 26) and integrated with respect to source energy. A similar operation was performed for the unscattered component of radiation as a function of distance (Figure A.4). Figure A.5 shows the total r^2 flux per neutron emitted by the source as a function of distance for each of the selected threshold values. For the sake of comparison, sulfur data from Shot 10 (gunshot) of Operation Upshot-Knothole are plotted. The sulfur data were matched to the theoretical 2.5-Mev thres-

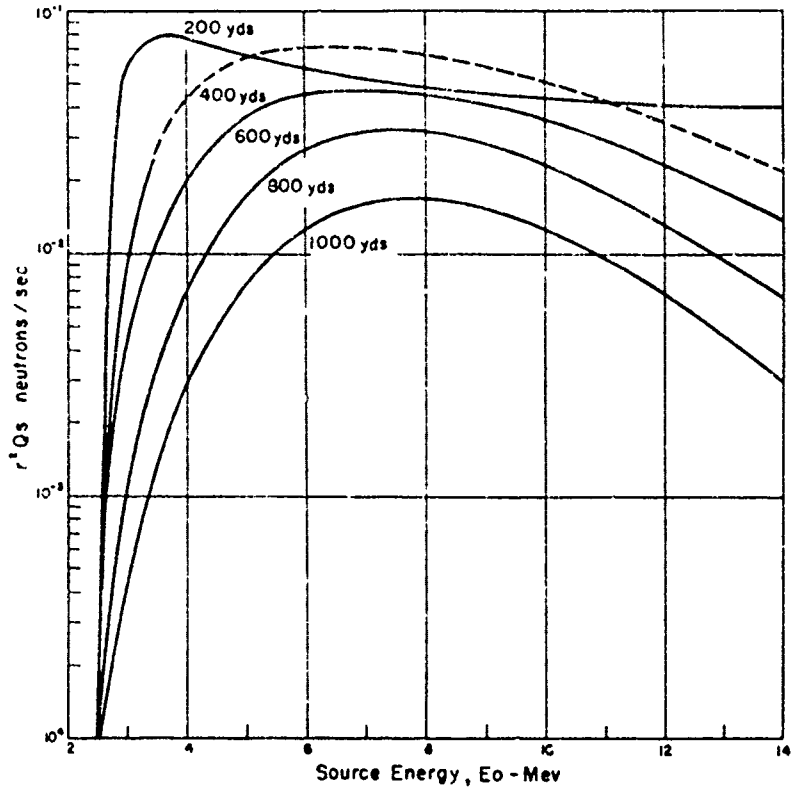

Figure A.3 Plot of scattered portion of the r^2 flux of neutrons with energy greater than 2.5 Mev from a monoenergetic point source, (emitting one neutron/sec) as a function of source energy at various distances from the source.

hold flux at about 600 yards, and the rest of the sulfur data multiplied by the same matching factor. It is seen that, except for points very near the source, the agreement is good.

A.3.2 Spectra. The spectra of neutrons emitted by a fission source in air were calculated at 200 and 1,000 yards using techniques similar to those cited above. The flux with arbitrary energy E at 200 and 1,000 yards was plotted as a function of source energy. These curves were then multiplied by the fission curve and integrated over source energy. The spectra are plotted in Figure A.6. For very small energies, it is seen that E^{-1} dependence is approached. This was to be expected on general theoretical grounds, since the scattering cross sections are relatively constant here and are nearly isotropic in their angular distribution. High energy variation of these curves is dominated by the fission-curve dependence.

The calculated spectra are compared with a spectrum measured by Handloser and Delihas (Reference 27) for degradation in graphite in Figure A.6. Although quantitative comparison is impossible because of the difference in media and the unknown effective distance of travel of the experimental scattered fission neutrons, the same E^{-1} dependence for low energies and the fission curve dominance at high energies can be seen.

A.3.3 Dose. Figure A.7 shows the variation with source energy of the scattered dose rate and its de-

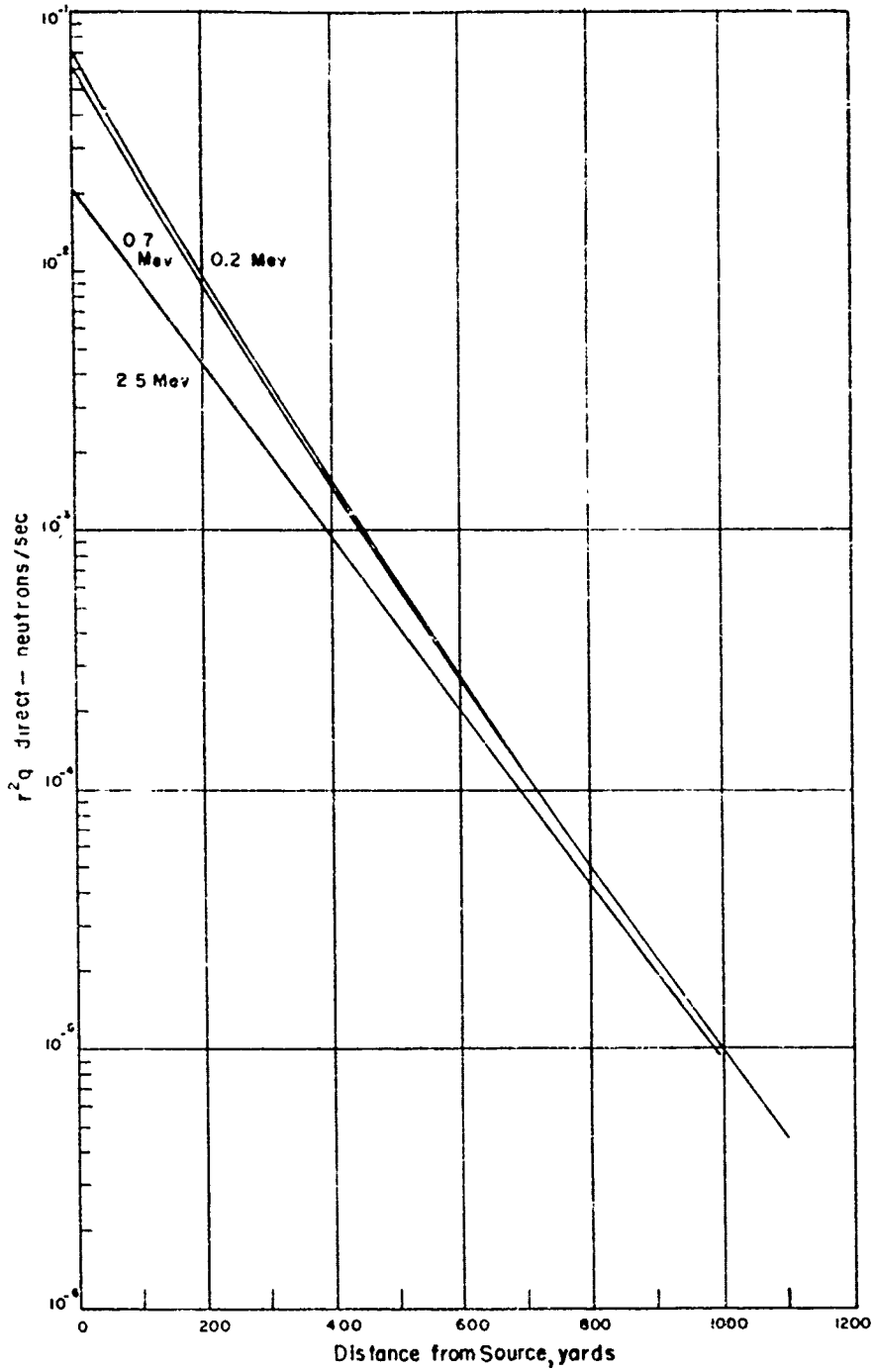

Figure A.4 Plot of r^2 flux of unscattered radiation greater than $E_{threshold}$ as a function of distance from a point-fission source.

pendence upon distance from an isotropic point source emitting one neutron per second. These curves were computed by multiplying spectra for the discrete monoenergetic sources by the dose weighting function given by Snyder and Neufeld (Reference 28). When weighted by the normalized fission spectrum and integrated over source energy, these curves yield the scattered dose rate as a function of distance for a fission source of unit strength. The total dose rate is obtained by adding in the direct dose rate obtained in a similar manner. The dependence of the dose rate on distance is plotted in Figure A.8.

A.3.4 Contribution of Source Energies to Flux. The normalized r^2 flux greater than 0.2 Mev is plotted as a function of source energy in Figure A.9. These curves show that, in spite of the relatively rapid decrease of the fission spectrum for high energies, the contribution from these high energies is dominant for distances greater than 600 yards.

A.4 DISCUSSION

A.4.1 Extent of Approximation. The data presented in this report are obtained from an approximate solution of the transport equation for a uniform infinite air space. The approximations involved are due

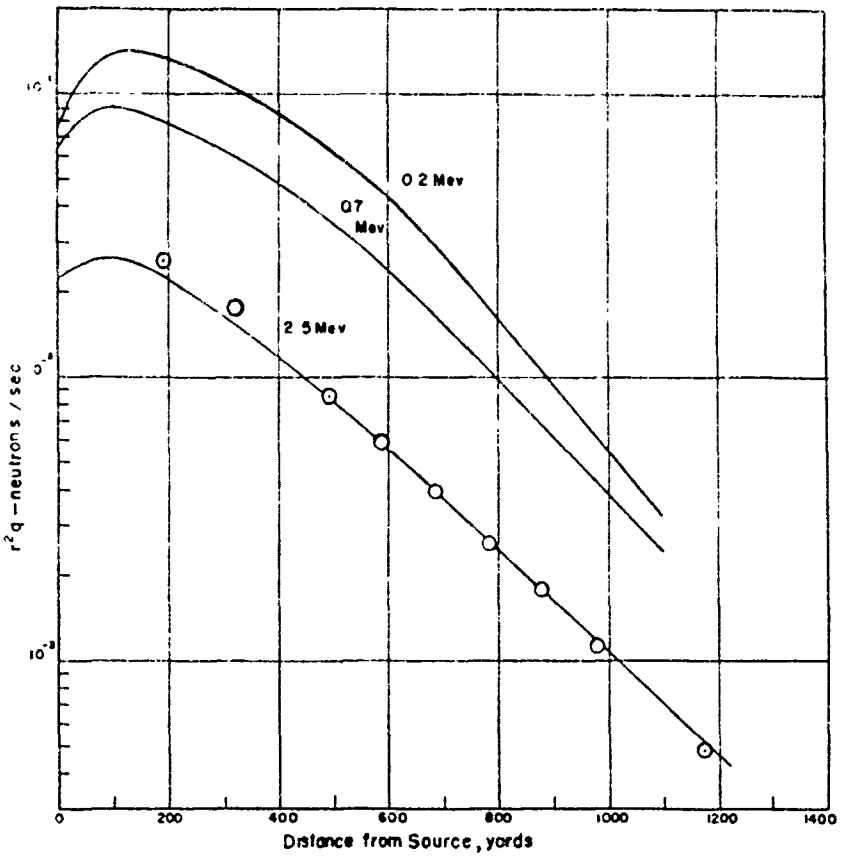

Figure A.5 Plot of total r^2 flux greater than $E_{threshold}$ from an isotropic point-fission source (emitting one neutron/sec) as a function of distance from the source. The points represent the gun-shot data of Operation Upshot-Knothole.

to the lack of complete information about the various cross sections of importance and to reconstruction of the flux from only a limited number of its moments.

There is, however, a more serious approximation introduced when these data are used to compare with field measurements of neutron fluxes. In an actual test shot, the fissionable material is surrounded by high explosives, steel casing, and possibly other materials, so that the original fission spectrum is perturbed to an unknown extent. Presumably the most effective ingredient of this surrounding material in perturbing the fission spectrum is hydrogen. In order to get a rough estimate of the extent of the change in source energy distribution, the spectrum of fission neutrons after being transported through 10 cm of

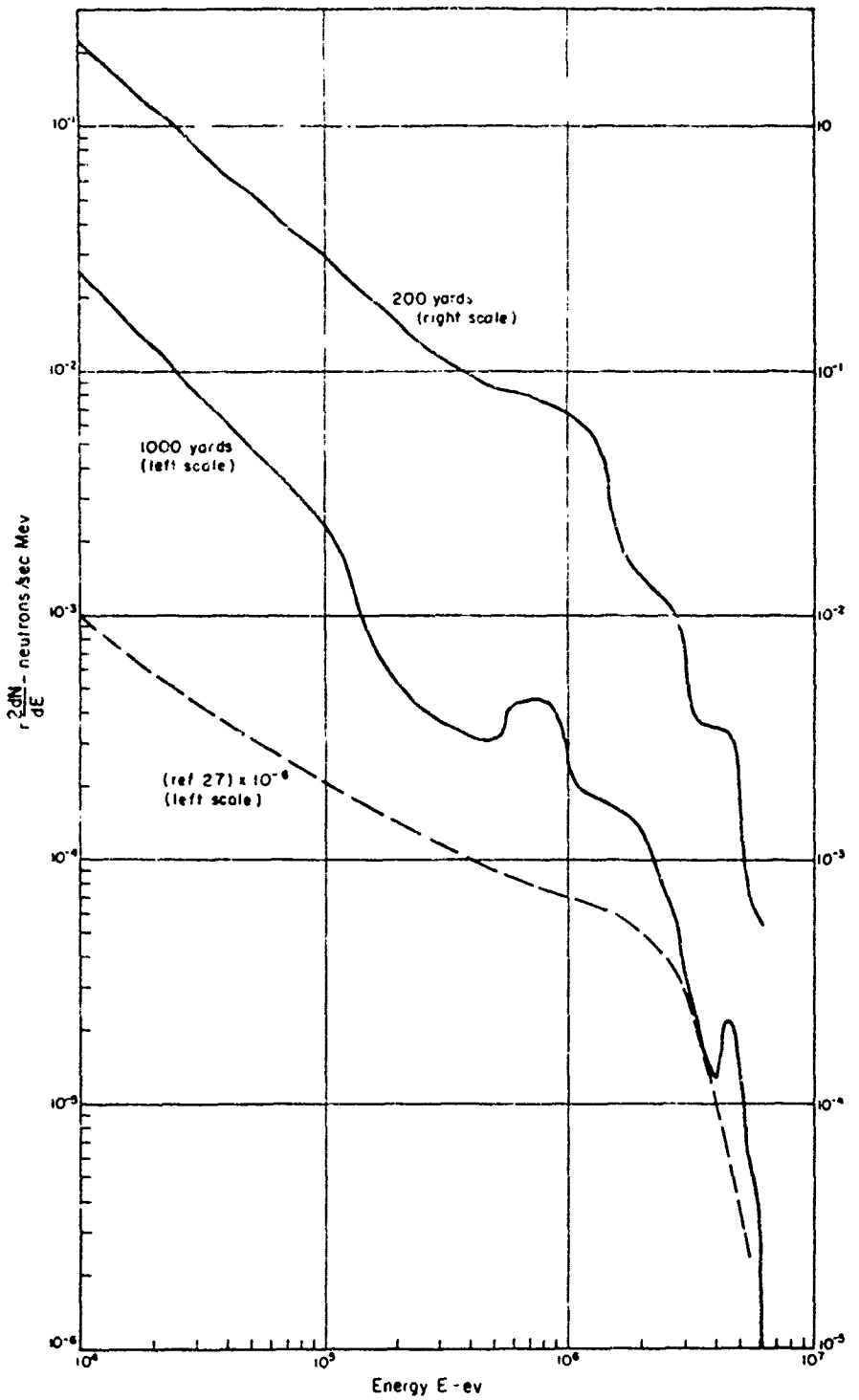

Figure A.6 Plot of r^2 number flux, $r^2 dn/dE$, from an isotropic fission source emitting one neutron/sec as a function of energy. The bottom curve is the data from Figure 8 of Reference 28.

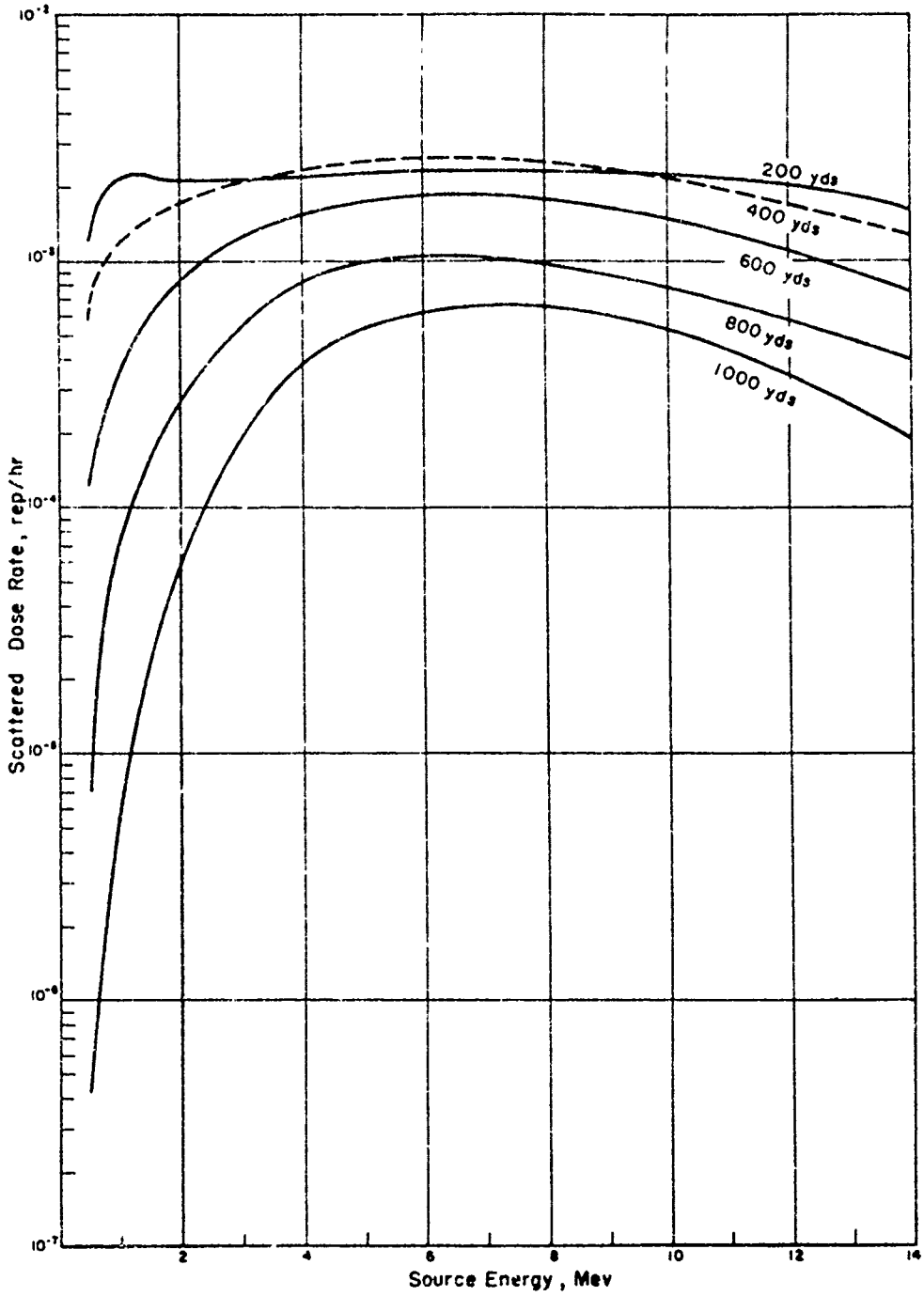

Figure A.7 Scattered dose rate as a function of source energy at several distances from a monoenergetic, isotropic point source emitting one neutron/sec.

water was obtained from Reference 29. The resulting spectrum differs only slightly from a fission shape for energies greater than about 0.5 Mev. The number of neutrons greater than 0.2 Mev was computed using the results in Reference 29 as a source spectrum, the spatial dependence was almost exactly the same as that for a fission source.

Perhaps a more-significant difficulty in comparing infinite-medium results to field data is due to the fact that all field measurements were made near the ground. In order to determine quantitatively the neutron flux as a function of distance, the effect of the ground as well as that of the bomb casing must be

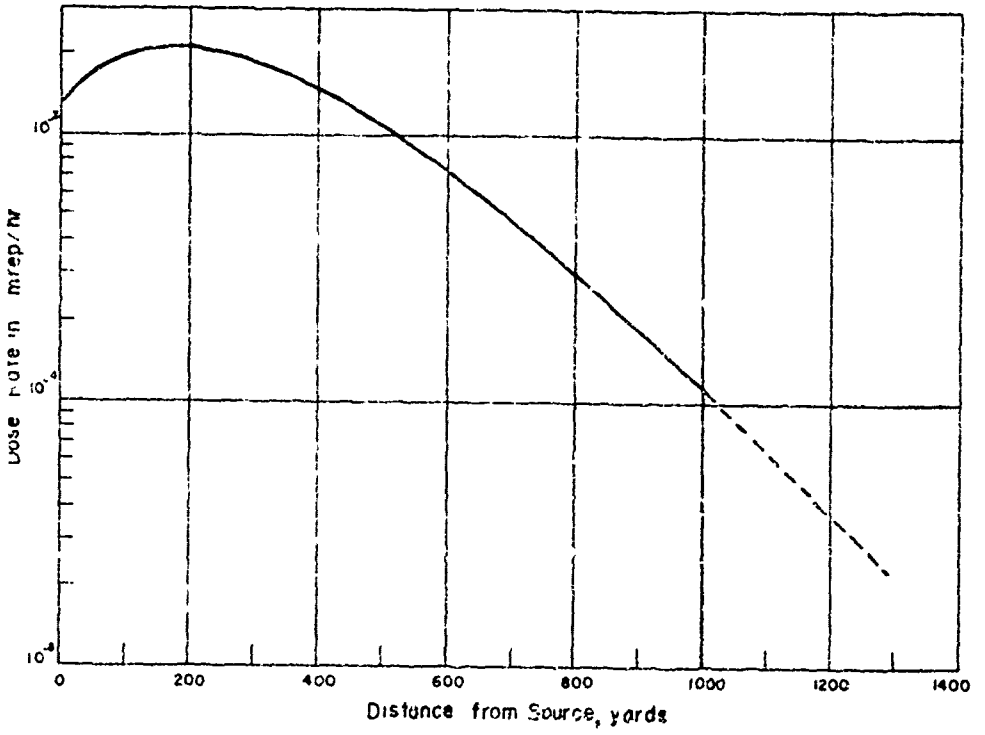

Figure A.8 Dose rate in mrep/hr as a function of distance in yards from a point isotropic fission source emitting one neutron/sec.

rigorously considered. However, certain conclusions of a qualitative nature may be drawn. For example, it was assumed that beyond a few mean free paths from the source the angular distribution of the flux becomes relatively fixed in an infinite air medium. Near the surface of the ground, then, it is expected that although the magnitude of the flux at each point is perturbed it will be multiplied by a constant factor at each point in space. Thus, within a few mean free paths of the source the spatial dependence of the flux under actual conditions of field geometry approaches that of the infinite air solution.

Finally, it should be pointed out that the theoretical results represent the actual r^2 flux greater than the selected threshold energies. This quantity may differ somewhat from field data obtained with detectors having cross sections which are not step functions i.e.:

$$\sigma(E) = 0 \quad , \quad E < E_{threshold}$$
$$\sigma(E) = \sigma_0 \quad E \geq E_{threshold}$$

A.4.2 Spatial Dependence. One of the most significant results of the evaluation of variation of the r^2 flux with distance is that considerable curvature exists in this function within the range of 0 to 1,000 yards. There is, in fact, a peak in this function at about 200 yards for all three detectors. Field-detector data for previous nuclear tests tend to verify this theoretical result in some cases, though data taken within 400 yards of a burst are generally sparse.

The analytical reasons for such behavior are clear. As mentioned in Reference 23, the r-dependence of the scattered flux becomes Gaussian within a few mean free paths of the source. The trial functions in Reference 23 for the r^2 flux at various energies, the use of which is justified ultimately by their compat-

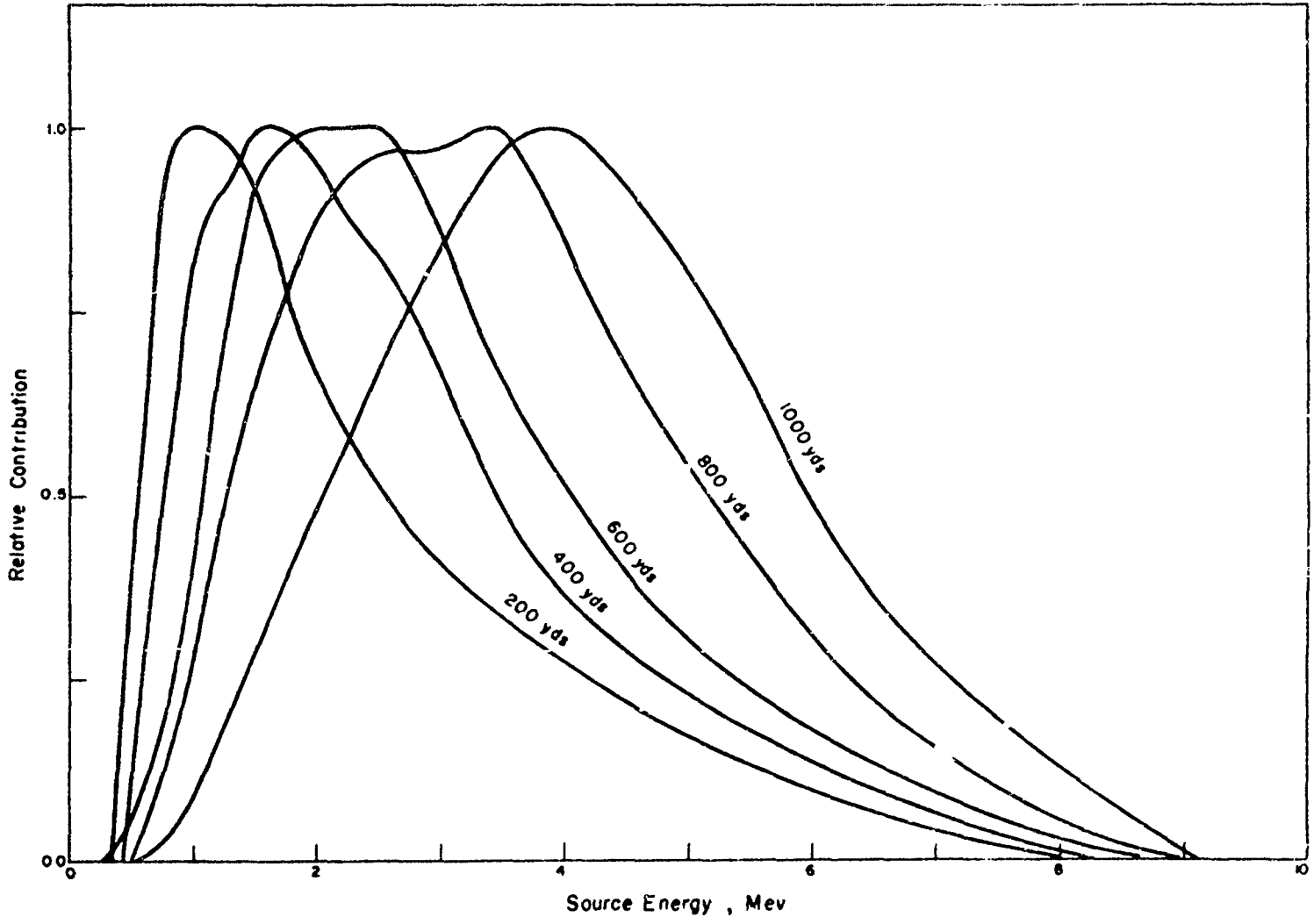

Figure A.9 Normalized flux greater than 0.2 Mev contributed at various distances as a function of source energy (fission source).

ibility with moments computed from the transport equation, generally have peaks within the range of one to two mean free paths from the origin. On the other hand, the scattered flux can be shown to have at most a $1/r$ singularity near the origin so that the function r^2 (scattered flux) must vanish at $r = 0$. The change in sign of $d/dr(r^2Q)$ near the origin is due to the quite-rapid decrease of the scattered contribution to r^2Q near the origin, where:

$$Q = \int_{4\pi} N(r, u, \cos\theta) \sin\theta \, d\theta \, dQ$$

Beyond 1,000 yards, r^2Q for the three detectors should be almost logarithmically linear with about as much curvature as shown for the unscattered contribution in Figure A.4. This is due to asymptotic dependence, xe^{-x} (Reference 23), except for each energy component of the scattered neutrons, which for large distances becomes as logarithmically linear as e^{-x}. The slopes, however, of direct and scattered contributions will not be the same in general, as can be seen from the development of Reference 23. The scattered portion, of course, will remain dominant in magnitude.

The above discussion points out the error in extrapolating experimental data (obtained in the quasi-linear portion of these curves) linearly to $r = 0$ in an effort to obtain the spectrum at the source and, perhaps, the attenuation due to the bomb casing.

In some cases, this fundamental fallacy has become apparent to data handlers, since the linearly extrapolated curves indicate a significantly greater number of neutrons at the origin than were calculated on the basis of the number of fission reactions

A.4.3 Proposed Theoretical Techniques. Though a completely rigorous technique to handle the transport of neutrons through the bomb casing, air, and earth is not available at present, it appears that techniques may be utilized which would give a better estimate of the neutron flux in this complicated geometry. A method has been suggested (Reference 30) whereby the geometry consisting of an isotropic point source arbitrarily located in a composite medium of two infinite half-spaces differing only in the density of scattering points, may be handled rigorously by a modification of the moment method. In order to obtain an equivalent source spectrum and its magnitude, it would be necessary to conduct Monte-Carlo computations of the outgoing neutrons from symmetrical bombs with varied parameters. The combination of Monte-Carlo results with the modified moment method would then yield rigorous results in the event that the cross sections in the upper half space were proportional to the corresponding ones in the lower half space at all energies, with the same constant of proportionality. Even if the above conditions were not exactly fulfilled, the use of this technique would presumably yield a better approximation, which takes into account, to some extent, the presence of the discontinuity in media.

REFERENCES

1. W.A. Biggers and others; "External Neutron and Gamma Flux Measurements by Sample Activation"; Annex 1.5, Part II, Section 2, Operation Greenhouse, WT-114, 1951, Los Alamos Scientific Laboratory, Los Alamos, New Mexico; Secret Restricted Data.

2. W.A. Biggers and others; "External Neutron Measurements with Threshold Detectors"; Project 17.1, Operation Upshot-Knothole, WT-826, March 1955; Los Alamos Scientific Laboratory, Los Alamos, New Mexico; Secret Restricted Data.

3. T.D. Hanscome and others; "Neutron Flux Measurements", Project 2.3, Operation Castle, WT-914, October 1955; Naval Research Laboratory, Washington, D.C., Secret Restricted Data.

4. T.D. Hanscome and others; "Neutron Flux Measurements"; Project 2.2, Operation Teapot, WT-1116, July 1958; Naval Research Laboratory, Washington, D.C.; Secret Restricted Data.

5. P.S. Harris and others; "Physical Measurement of Neutron and Gamma Radiation Dose from High Neutron Yield Weapons and Correlation of Dose with Biological Effect"; Project 39.7, Operation Teapot, ITR-1167, April 1955; Civil Effects Test Group, Secret Restricted Data.

6. "Scientific Director's Report"; Operation Sandstone, Vol 18, Annex 4, Part I and Addendum, 1948; Secret Restricted Data.

7. W. Ogle and others, "Neutron Measurements"; Operation Ranger, LASL Report LAB-J-2095; Secret Restricted Data.

8. T.D. Hanscome and others; "Neutron Flux Measurements", Project 2.3, Operation Snapper, WT-524, February 1953; Office of Naval Research, Naval Research Laboratory, Washington, D.C., Secret Restricted Data.

9. C.L. Cowan and others; "External Neutron Measurements"; Project 10.8, Operation Buster-Jangle, WT-416, June 1952, Los Alamos Scientific Laboratory, Los Alamos, New Mexico; Secret Restricted Data.

10. H.E. Grier and others; "Program Reports, Weapons Development"; Vol 3, Operation Ranger, WT-203, 1951; Los Alamos Scientific Laboratory, Los Alamos, New Mexico; Secret Restricted Data.

11. D.K. Willett and others; "Neutron Flux Measurements"; Project 2.3, Operation Upshot-Knothole, WT-720, December 1953; Office of Naval Research, Naval Research Laboratory, Washington, D.C.; Secret Restricted Data.

12. W.A. Biggers and others; "External Neutron Measurements"; Project 14.1, Operation Castle, WT-952, October 1955; Los Alamos Scientific Laboratory, Los Alamos, New Mexico; Secret Restricted Data.

13. G.S. Hurst, R.H. Richie, and H.N. Wilson; Sci Instr 22, 981, 1951; Unclassified.

14. G.S. Hurst and others; "Techniques of Measuring Neutron Spectrum with Threshold Detectors, Tissue Dose Determination"; Oak Ridge National Laboratory, Oak Ridge, Tennessee, (to be published) Unclassified.

15. B. Cassen and others; "Measurement of Fast Neutrons by Effects on Semiconductors"; Project 29.2, Operation Upshot-Knothole, WT-803, September 1953; School of Medicine, Atomic Energy Project, University of California at Los Angeles and North American Aviation, Inc., Los Angeles, California; Confidential Restricted Data.

16. B. Cassen and others, "Measurement and Permanent Recording of Fast Neutrons by Effects on Semiconductors"; Project 39.5, Operation Teapot, ITR-1179, May 1955; School of Medicine, Atomic Energy Project, University of California at Los Angeles; Confidential Restricted Data.

17. Hughes and Schwartz; "Neutron Cross Sections"; Second Edition, Brookhaven National Laboratory, July 1958.

18. J. Allred and others; "Greenhouse Neutron Measurements"; Preliminary Report of Group LAJ-3, 1951; Los Alamos Scientific Laboratory, Los Alamos, New Mexico; Secret Restricted Data.

19. Sigoloff, Borella, and Auxier; "Dosimetry Report, Biological Effects from Massive Doses of Neutron-Gamma Radiation"; USAF Report No. 55-108; School of Aviation Medicine, Randolph Field, Texas.

20. S.C. Sigoloff; "Fast Neutron Insensitive Gamma Ray Dosimeters, the AC and ATCE Systems"; School of Aviation Medicine, Randolph Field, Texas (in press).

21. G.V. Taplin and others; "Comparison and Evaluation of Dosimetry Methods Applicable to Gamma Radiation"; Project 29.1, Operation Upshot-Knothole, WT-802, 1953; School of Medicine, Atomic Energy Project, University of California at Los Angeles; Confidential Restricted Data.

22. G.V. Taplin; "Measurement of Initial and Residual Radiation by Chemical Methods"; Project 39.6, Operation Teapot, ITR-1171, May 1955; School of Medicine, Atomic Energy Project, University of California at Los Angeles; Secret Restricted Data.

23. S.S. Holland and P.I. Richards; "Penetration of Neutrons in Air"; AFSWC-TR-55-27, 1955; Unclassified.

24. H. Goldstein and J.E. Wilkins; "Calculation of Penetration of Gamma Rays"; NYO-3075, 1954; Unclassified.

25. L.V. Spencer and U. Fano; "Journal of Research"; NBS-46, 446, 1951; Unclassified.

26. "Reactor Handbook"; Vol 1; AEC-3645, 1955; Unclassified.

27. J.S. Handloser and N. Delihas; BNL-386 (T-72), 1955; Unclassified.

28. Snyder and Neufeld; WASH-95, 1952; Unclassified.

29. R. Aronson and others; "Penetration of Neutrons from a Point Isotropic Fission Source in Water"; NYO-6267; Unclassified.

30. S.S. Holland; private communication.

31. J.D. Seagrave; "D(d, n) He^3 and T(d, n) He^4 Source Handbook"; LAMS-2162, 1957; Unclassified.

32. J.W. Kinch and D.L. Rigotti; "An Activation Type Neutron Detection System and Its Calibration"; Technical Report (to be published); U.S. Army Chemical Warfare Laboratories, Army Chemical Center, Maryland; Confidential Formerly Restricted Data.